Fog- and cloud-induced aerosol modification observed by the Aerosol Robotic Network (AERONET)

T. F. Eck,[1,2] B. N. Holben,[2] J. S. Reid,[3] D. M. Giles,[2,4] M. A. Rivas,[5] R. P. Singh,[6] S. N. Tripathi,[7] C. J. Bruegge,[8] S. Platnick,[2] G. T. Arnold,[2,9] N. A. Krotkov,[2] S. A. Carn,[10] A. Sinyuk,[2,4] O. Dubovik,[11] A. Arola,[12] J. S. Schafer,[2,4] P. Artaxo,[13] A. Smirnov,[2,4] H. Chen,[14] and P. Goloub[11]

Received 6 September 2011; revised 10 February 2012; accepted 12 February 2012; published 5 April 2012.

[1] Large fine mode–dominated aerosols (submicron radius) in size distributions retrieved from the Aerosol Robotic Network (AERONET) have been observed after fog or low-altitude cloud dissipation events. These column-integrated size distributions have been obtained at several sites in many regions of the world, typically after evaporation of low-altitude cloud such as stratocumulus or fog. Retrievals with cloud-processed aerosol are sometimes bimodal in the accumulation mode with the larger-size mode often ~0.4–0.5 μm radius (volume distribution); the smaller mode, typically ~0.12 to ~0.20 μm, may be interstitial aerosol that were not modified by incorporation in droplets and/or aerosol that are less hygroscopic in nature. Bimodal accumulation mode size distributions have often been observed from in situ measurements of aerosols that have interacted with clouds, and AERONET size distribution retrievals made after dissipation of cloud or fog are in good agreement with particle sizes measured by in situ techniques for cloud-processed aerosols. Aerosols of this type and large size range (in lower concentrations) may also be formed by cloud processing in partly cloudy conditions and may contribute to the "shoulder" of larger-size particles in the accumulation mode retrievals, especially in regions where sulfate and other soluble aerosol are a significant component of the total aerosol composition. Observed trends of increasing aerosol optical depth (AOD) as fine mode radius increased suggests higher AOD in the near-cloud environment and higher overall AOD than typically obtained from remote sensing owing to bias toward sampling at low cloud fraction.

Citation: Eck, T. F., et al. (2012), Fog- and cloud-induced aerosol modification observed by the Aerosol Robotic Network (AERONET), *J. Geophys. Res.*, *117*, D07206, doi:10.1029/2011JD016839.

1. Introduction

[2] Aerosol interactions with clouds are currently the largest source of uncertainty in assessment of the anthropogenic aerosol radiative forcing on climate [*Intergovernmental Panel on Climate Change* (*IPCC*), 2007]. This pertains primarily to how aerosols modify cloud properties such as albedo [*Twomey*, 1977] and lifetime [*Albrecht*, 1989], and for absorbing aerosol particles the semidirect effect of suppression of convection [*Hansen et al.*, 1997; *Koren et al.*, 2004]. However, the related modification of aerosol properties by interaction with clouds is also of significant importance in accurately assessing aerosol evolution and direct radiative forcing. Globally the majority of aerosol particles are located in the planetary boundary layer (typically lowest 1–3 km), therefore when low-altitude nonprecipitating clouds (or fog) are coincident with or interact with this aerosol layer then the potential for cloud-aerosol interactions is maximized. Aerosol particles may be modified by clouds from hygroscopic growth in high relative humidity conditions within the cloud, or in the near-cloud enhanced humidity environment [*Radke and Hobbs*, 1991]. Additionally, aerosol particles may serve

[1]Universities Space Research Association, Columbia, Maryland, USA.
[2]NASA Goddard Space Flight Center, Greenbelt, Maryland, USA.
[3]Naval Research Laboratory, Monterey, California, USA.
[4]Sigma Space Corporation, Lanham, Maryland, USA.
[5]Laboratorio de Radiación Solar Ultravioleta, Departamento de Física, Facultad de Ciencias, Universidad de Tarapacá, Arica, Chile.
[6]School of Earth and Environmental Sciences, Chapman University, Orange, California, USA.
[7]Department of Civil Engineering, Indian Institute of Technology Kanpur, Kanpur, India.
[8]NASA Jet Propulsion Laboratory, Pasadena, California, USA.
[9]Science Systems Applications, Inc., Lanham, Maryland, USA.
[10]Department of Geological and Mining Engineering and Sciences, Michigan Technological University, Houghton, Michigan, USA.
[11]Laboratoire d'Optique Atmospherique, CNRS, Universite de Lille, Villeneuve d'Ascq, France.
[12]Finnish Meteorological Institute, Kuopio, Finland.
[13]Institute of Physics, University of São Paulo, São Paulo, Brazil.
[14]Institute of Atmospheric Physics, Chinese Academy of Sciences, Beijing, China.

0148-0227/12/2011JD016839

as cloud condensation nuclei (CCN) and subsequent aqueous phase chemistry may result in modified aerosol properties of the particles that remain after evaporation of the cloud droplet; that is, cloud-processed aerosols [*Hoppel et al.*, 1994; *Alkezweeny*, 1995; *Lelieveld and Heintzenberg*, 1992; *Lu et al.*, 2003; *Hegg et al.*, 2004]. Those particles that have served as CCN and subsequently exhibited an increase in size and mass are also sometimes called cloud residue. Furthermore, new particle formation has also been observed in cloud environments [*Hoppel et al.*, 1994]. Ultimately the processing of aerosol particles in clouds results in larger particle sizes and increased soluble components.

[3] Several recent studies suggest changes in aerosol optical properties by clouds or in the vicinity of clouds. *Twohy et al.* [2009] analyzed in situ aircraft data from INDOEX over the northern Indian Ocean and found relative humidity increased within ~1 km of small low-altitude marine cumulus, and this resulted in increases of about 40–80% in aerosol scattering as a result of hygroscopic growth. *Li et al.* [2011] made in situ measurements of aerosols from a mountain observatory at ~1.5 km altitude in northeastern China during 4 days in April 2010. Their observations were made under highly polluted aerosol conditions and found significantly larger radius for cloud residue aerosols versus interstitial aerosol (~0.22 μm versus ~0.4 μm, for number size distributions), and the number of particles decreased by ~50% during cloud formation demonstrating how efficiently aerosol particles were incorporated into cloud droplets. They also found that ~92% of the cloud residue particle composition was dominated by sulfate and soluble organic matter salts. *Zhang and Tie* [2011] measured 75% conversion of sulfur dioxide from gas to aqueous phase during a fog event in polluted conditions, in the same region of northeastern China, suggesting that SO_2 has greater solubility than had been previously thought.

[4] Several studies have used lidar observations to investigate the aerosol environment in the proximity of clouds. *Su et al.* [2008] used HSRL lidar from aircraft to investigate the near-cloud aerosol environment for three cases of low-altitude clouds (<3 km). They found enhancement of aerosol optical depth (AOD) by ~8–17% within ~100 m of clouds in comparison to measurements made 4.5 km from clouds. They suggest that the observed increases in backscatter and extinction coefficients near clouds could be explained by both humidification and cloud processing of aerosols. Analysis of satellite lidar data from CALIPSO by *Tackett and DiGirolamo* [2009] showed enhanced backscatter near to the cloud edge for western Atlantic trade wind cumulus (single layer), which they suggested was best explained by increased aerosol radius and reduced number size distribution. Additionally, an analysis of CALIPSO data over oceans by *Várnai and Marshak* [2011] found increased backscatter and increased particle size in a transition zone of ~15 km around clouds over all oceans, with near-cloud enhancements strongest at low altitudes.

[5] An analysis of the relationship between cloud fraction and AERONET direct Sun measurements of AOD, for a site in the U.S. Great Plains region (Oklahoma) was carried out by *Jeong and Li* [2010]. Their study showed increasing AOD as cloud fraction increased, with only about 25% of the increase attributed to humidification, while the bulk of the increase was likely due to a combination of cloud processing of aerosols, new particle genesis and atmospheric dynamics. Additionally, they also found that in situ aircraft measured AOD (vertically integrated extinction coefficients) at the same site and time interval also showed increasing AOD as cloud cover increased, thereby reducing the possibility that any significant amount of the Sun photometer measured increases in AOD as a function of cloud fraction were due to cloud contamination.

[6] In the current study we analyze aerosol size distribution retrievals from almucanatar scans made by AERONET Sun-sky radiometers in specific situations where extensive fog or low-altitude cloud layers have recently dissipated (evaporated). These are cases where at least a portion of both the aerosol layer and fog/cloud layer were coincident in vertical profile thereby resulting in significant probability for cloud-aerosol interaction. Cases from many different regions of the world are shown for interaction between primarily pollution (urban-industrial type) aerosols and cloud or fog.

2. Instrumentation and Methodology

2.1. AERONET Instrumentation

[7] The CIMEL Electronique CE-318 Sun-sky radiometer measurements were made with instruments that are a part of the Aerosol Robotic Network (AERONET) global network. These instruments are described in detail by *Holben et al.* [1998]; however, a brief description is given here. The automatic tracking Sun and sky scanning radiometers made direct Sun measurements with a 1.2° full field of view every 15 min at 340, 380, 440, 500, 675, 870, 940, and 1020 nm (nominal wavelengths). However, for the Beijing site the version of the CIMEL installed there most years had only the 440, 675, 870 and 1020 nm channels for AOD measurement. The direct Sun measurements take ~8 s to scan all 8 wavelengths (repeated three times within a minute), with a motor driven filter wheel positioning each filter in front of the detector. These solar extinction measurements are used to compute aerosol optical depth (AOD or τ_a) at each wavelength except for the 940 nm channel, which is used to retrieve total column water vapor (or precipitable water) in centimeters. The filters utilized in these instruments were ion assisted deposition interference filters with band pass (full width at half maximum) of 10 nm, except for the 340 and 380 nm channels at 2 nm. The estimated uncertainty in computed τ_a, due primarily to calibration uncertainty, is ~0.010–0.021 for field instruments (which is spectrally dependent with the higher errors in the UV) [*Eck et al.*, 1999]). *Schmid et al.* [1999] compared τ_a values derived from 4 different solar radiometers (including an AERONET Sun-sky radiometer) operating simultaneously together in a field experiment and found that the τ_a values from 380 to 1020 nm agreed to within 0.015 (RMS), which is similar to our estimated level of uncertainty in τ_a retrieval for field instruments. Only AERONET version 2 level 2 AOD data have been analyzed, unless otherwise specified. The spectral aerosol optical depth data have been screened for clouds following the methodology of *Smirnov et al.* [2000], which relies on the higher temporal frequencies of cloud optical depth versus aerosol optical depth. The sky radiances measured by the Sun/sky radiometers are calibrated versus frequently characterized integrating spheres at the NASA

Goddard Space Flight Center, to an absolute accuracy of ~5% or better [*Holben et al.*, 1998].

2.2. Inversion Methodology

[8] The CIMEL sky radiance measurements in the almucantar geometry (fixed elevation angle equal to solar elevation and a full 360° azimuthal sweep) at 440, 675, 870, and 1020 nm (nominal wavelengths) in conjunction with the direct Sun measured τ_a at these same wavelengths were used to retrieve optical equivalent, column integrated aerosol size distributions and refractive indices. Using this microphysical information the spectral dependence of single scattering albedo is calculated. The algorithm of *Dubovik and King* [2000] with enhancements detailed in the work of *Dubovik et al.* [2006] was utilized in these retrievals, known as version 2 AERONET retrievals. Only version 2 and level 2 quality assured retrievals [*Holben et al.*, 2006] are presented in this paper, unless otherwise noted. The version 2 AERONET algorithm determines the percentage of spherical and spheroidal particles required to give the best fit to the measured spectral sky radiance angular distribution. Further details on the version 2 algorithm and the improved specification of surface bidirectional reflectance can be found in the work of *Dubovik et al.* [2006] and *Eck et al.* [2008].

[9] Almucantar sky radiance measurements were made at optical air masses of 4, 3, 2, and 1.7 (75, 70, 60, 54 degrees solar zenith angle, respectively) in the morning and afternoon, and once per hour in between. In order to ensure sky radiance data over a wide range of scattering angles, only almucantar scans at solar zenith angles greater than ~50 degrees are analyzed and presented here. To eliminate cloud contamination from the almucantar directional sky radiance data AERONET requires the radiances to be symmetrical on both sides of the Sun at equal scattering angles, and symmetric radiances from both sides are subsequently averaged. Directional sky radiance measurements that are not symmetrical (owing to cloud on one side or inhomogeneous aerosol distribution) are eliminated, and the minimum number of measurements required in given scattering angle ranges for a level 2 retrieval are shown in the work of *Holben et al.* [2006]. The stable performance of the inversion algorithm was illustrated in sensitivity studies performed by *Dubovik et al.* [2000] where the perturbations of the inversion resulting from random errors, possible instrument offsets and known uncertainties in the atmospheric radiation model were analyzed. Their work employed retrieval tests using known size distributions to demonstrate successful retrievals of mode radii and the relative magnitude of modes for various types of bimodal size distributions such as those dominated by a submicron accumulation mode or distributions dominated by supermicron coarse mode aerosols. Although very few direct comparisons of size distribution between in situ and AERONET retrievals have been made there are several aerosol types in specific regions that have been or can be compared. For example, *Reid et al.* [2005] presents a table were the volume median radius of smoke from various major biomass burning regions (South America, southern Africa, North America (boreal, temperate)) are compared. For all three of these regions, the volume median diameters of the in situ versus the AERONET retrievals are often within ~0.01 μm of each other. Similarly, for fine mode pollution in the Arabian Sea during INDOEX, *Clarke et al.* [2002] presented lognormal fits of volume size distributions from aircraft and ship in situ instrument measurements that showed average accumulation mode volume peak radius values of 0.17 μm to 0.18 μm with geometric standard deviations of 1.43 (aircraft) and 1.51 (ship) for observations made under high aerosol scattering conditions. This compares well with retrievals made at Kaashidhoo Island, Maldives (in the same region), when AOD (440 nm) >0.4, of 0.18 μm median radius and width of 1.49 (AERONET version 2 averages from 1998 to 2000). For larger submicron-sized aerosols, *Eck et al.* [2010] discussed the relatively close agreement for Pinatubo stratospheric aerosol observations of ~0.56 μm peak volume radius from AERONET retrievals to 0.53 μm effective radius from in situ stratospheric aircraft measurements, as reported by *Pueschel et al.* [1994]. In the coarse mode (supermicron radius), *Reid et al.* [2006, 2008] showed excellent agreement between in situ measured size and AERONET retrievals for sea salt and desert dust, respectively. Similarly, *Johnson and Osborne* [2011] have shown good agreement between aircraft in situ measured size distributions and AERONET retrievals for coarse mode dust in the Sahel region of West Africa.

3. Results and Discussion

3.1. Kanpur, India

[10] The Kanpur AERONET site in India is located immediately to the northwest of Kanpur, an industrial city with population ~5 million in 2009. The Indo-Gangetic Plain region where Kanpur is located is a major emission source of pollution aerosol from the combustion of fossil fuels and biofuels [*Singh et al.*, 2004; *Novakov et al.*, 2000; *Venkataraman et al.*, 2005; *Prasad et al.*, 2006]. Also in spring and early summer the aerosol type variation at Kanpur was strongly influenced by desert dust advected eastward from arid and semiarid lands in India and Pakistan and from arid regions farther west in the Middle East [*Dey et al.*, 2004; *Chinnam et al.*, 2006; *Prasad and Singh*, 2007; *Gautam et al.*, 2009]. Analysis of aerosol fine mode fraction (FMF) of AOD versus Angstrom exponent (440–870 nm) from a previous paper [*Eck et al.*, 2010] for Kanpur, India showed a multiyear (2002–2006) climatology based on almucantar retrievals of FMF. As identified in Figure 1, there is a small cluster of outlier observations (7 days out of 591 days total) that have relatively low Angstrom exponent (<1.0) at high fine mode fraction of AOD (>0.90 at 440 nm). All of the outlier cases in this plot occurred during the month of January, when fine mode pollution aerosols dominate [*Eck et al.*, 2010]. When these dates were examined in detail, it was observed for all of these cases that MODIS satellite images showed low cloud or fog (fog is cloud that extends to Earth's surface) either over or near to the Kanpur site location at the time of the morning Terra satellite overpass, with the fog/cloud having dissipated or partially dissipated by the time of the early afternoon Aqua satellite overpass. It is well known that fog frequently occurs in the Indo-Gangetic plain in the winter months and is typically associated with high aerosol concentrations [*Jenamani*, 2007; *Gautam et al.*, 2007; *Badarinath et al.*, 2009; *Tripathi et al.*, 2006; *Tare et al.*, 2006; *Baxla et al.*, 2009],

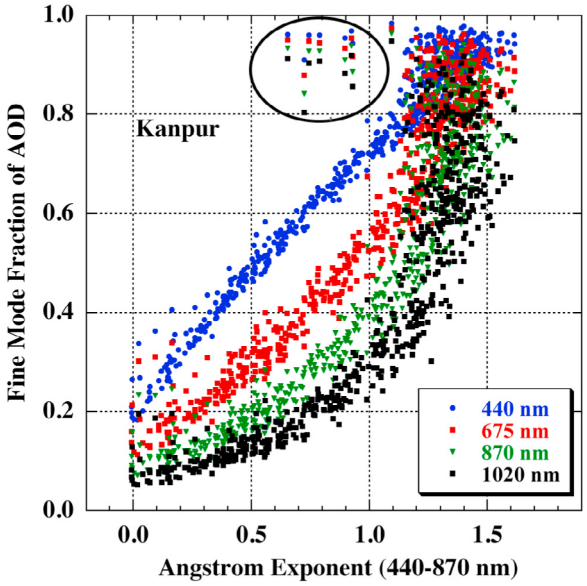

Figure 1. Daily averages of spectral fine mode fraction of AOD (from the Dubovik algorithm almucantar retrievals) versus Angstrom exponent (440–870 nm) at Kanpur, India, for the years 2002–2006 [from *Eck et al.*, 2010]. Circled are the outlier values of relatively low Angstrom exponent (<1.0) and high fine mode fraction (>0.90 at 440 nm) that were all observed during the month of January.

affecting the lives of millions of people in the region through the cancellation of flights, late running trains, and poor visibility. MODIS satellite images for one of these cases, 5 January 2006, are shown in Figure 2. Weather station observations obtained from Russia's Weather Server–Weather Archive (http://meteo.infospace.ru/wcarch/html/index.sht) on this date from nearby Lucknow (~60 km northeast of Kanpur) indicated patches of shallow fog with 94% surface relative humidity and 0.5 km visibility at 03:00 UTC, and at 06:00 UTC mist was observed with cloud base height at 150 m and 90% cloud cover, while there were no clouds noted from 09:00 through 18:00 UTC. On this day satellite imagery shows that an extensive area of bright white cloud/fog is located immediately adjacent and to the north of the Kanpur site at the Terra overpass time of 05:15 UTC while most of this fog/cloud has dissipated by about 08:20 UTC (3 h later) at the time of the Aqua overpass. A relatively uniform gray haze is seen in the Aqua image in the region surrounding Kanpur after the dissipation of the fog/cloud. The fog/clouds that have not evaporated in this image are 100 km or more to the north and northeast, and therefore much too far to be observed in the direct Sun AOD measurements or in the almucantar sky radiance scans made after the Aqua overpass time.

[11] The cloud screened spectral AOD observations for this day show that AOD (440 nm) was ~0.60. The two almucantar retrievals (level 2.0) were made at 08:37 UTC and 10:06 UTC, when the Angstrom exponent (440–870 nm) was ~0.84 and ~1.0, respectively. The aerosol volume size distribution retrievals from these two almucantar scans are shown in Figure 3. The bimodal nature of the accumulation mode (radius <1 micron) seen in these cases is not very commonly observed in AERONET retrievals. Exceptions include aged volcanic aerosol in the stratosphere (from Mt. Pinatubo, for example) and sometimes dust from certain source regions such as the Bodele depression, which both had a volume distribution mode peak radius of ~0.60 micron [*Eck et al.*, 2010]. The larger mode in this Kanpur case shows a peak radius of ~0.45 microns, with the smaller of the two accumulation modes peaking at ~0.15 to 0.20 microns. It is noted that the coarse mode AOD (computed from

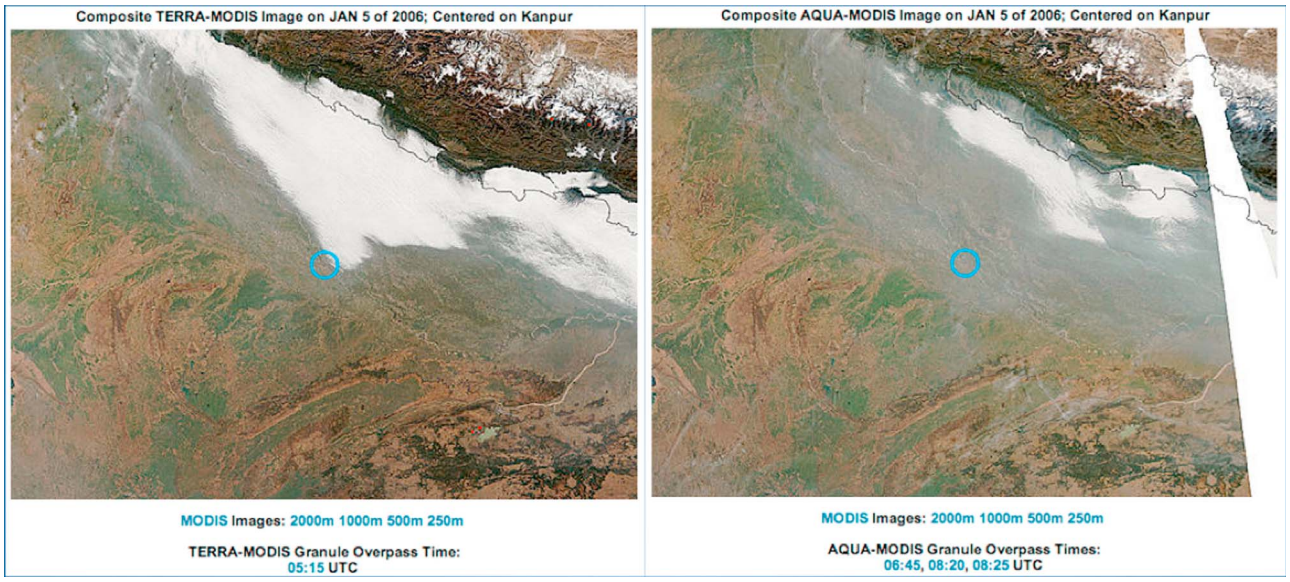

Figure 2. MODIS satellite images centered on the Kanpur, India, site (blue circles) from 5 January 2006. The morning (05:15 UTC) Terra image shows fog/cloud adjacent and to the north of Kanpur, and the afternoon (~08:20 UTC) Aqua image shows only haze in the vicinity of Kanpur, with fog having dissipated except in the northern Indo-Gangetic Plain bordering Nepal. (Image courtesy of NASA/Goddard Space Flight Center Rapid Response.)

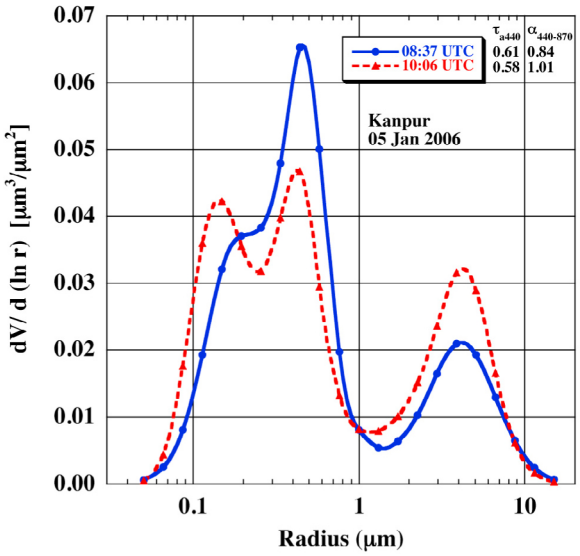

Figure 3. Almucantar retrievals of the aerosol volume size distribution at Kanpur on 5 January 2006 at 08:37 UTC (only 17 min after the Aqua MODIS image in Figure 2) and at 10:06 UTC. Note the bimodality of the submicron radius mode.

radius >0.99 μm) for these retrievals is only 0.015 to 0.022 (wavelength independent), relatively insignificant compared to the fine mode AOD, and therefore suggesting that there was no cloud contamination owing to this low coarse mode AOD. Cloud contamination in AERONET retrievals results in size distribution enhancement of aerosols with peak radius of ~1 to 6 μm, therefore much larger than the 0.4 to 0.5 μm size particles attributed to cloud processing of aerosol. In situ measured aerosol size distributions have shown bimodality of the accumulation mode in cases where at least some of the particles have been cloud processed. *Hoppel et al.* [1994] measured aerosol number size distributions from an airship in close proximity to a stratus cloud deck off of the coast of Oregon. These size distributions exhibited a distinct bimodality in the accumulation mode that Hoppel *et al.* attributed to cloud processing of aerosols and in-cloud conversion of sulfur dioxide gas to sulfate particles, which formed the larger of the two modes, and the interstitial aerosols (not interacting with cloud) comprising the smaller of the modes. *Das et al.* [2008] also measured bimodal submicron aerosol size distributions and an increase in accumulation mode radius for aerosols that had interacted with fog in the Indo-Gangetic Plain of India. In Figure 3 it is seen that the size distribution retrieved closer to the time of the fog dissipation (evaporation) shows a greater contribution of the ~0.45 μm radius mode than retrieved ~1.5 h later, perhaps owing to decay or dissipation of the cloud-processed aerosol, and conversely a larger contribution (and smaller radius) of the interstitial aerosol mode perhaps owing to drying of humidified aerosol and emission and/or creation of fresh aerosols. The smaller of the two modes may also be aerosol that had no interaction with the fog, perhaps aerosol that was located at an altitude above the fog layer. *Dall'Osto et al.* [2009] measured ambient aerosol sizes in association with a fog event in London, and data for the largest mode measured are reproduced in Figure 4 (with additional conversion to volume distribution). The large particles shown in Figure 4 are composed of hydroxymethanesulphonate (HMS), which is a chemical species that is only formed in aqueous phase chemistry and therefore a valuable tracer for aerosol processing by cloud or fog. It is noted that the size of these HMS particles formed in the London fog event (peak volume radius of ~0.45–0.50 μm) are essentially the same as the larger of the two accumulation modes observed over Kanpur after fog dissipation (Figure 3).

[12] In addition to aerosol size distribution modification by fog/cloud interaction, the AERONET retrievals also suggest that the aerosol absorption properties are modified. Figure 5 shows the retrieved aerosol single scattering albedo (SSA) in visible wavelengths (440 and 675 nm) as a function of fine mode volume median radius for all almucanatar retrievals made during the month of January at the Kanpur site. There is a clear trend of increasing SSA as fine mode radius increases. The largest of these fine mode radius cases, with radius >0.25 μm, are mostly fog/cloud interaction cases, and show a nearly linear increase in SSA as radius increases. These larger-size, cloud-processed aerosols would likely contain more water and sulfate, both of which are non absorbing, and the increased radius of the aerosols also increases the scattering efficiency, thereby increasing the single scattering albedo. Figure 5 also shows that there is a distinct trend of increasing SSA as radius increases for aerosol of radius <0.25 μm, likely owing to particle growth by coagulation and hygroscopic growth, also resulting in more efficient scattering at larger radius in combination with either nearly constant or lower imaginary refractive index. The climatological average of SSA in winter at Kanpur is nearly spectrally flat [see *Eck et al.*, 2010], however, with variation of ±0.02 for the difference in SSA from 440 to

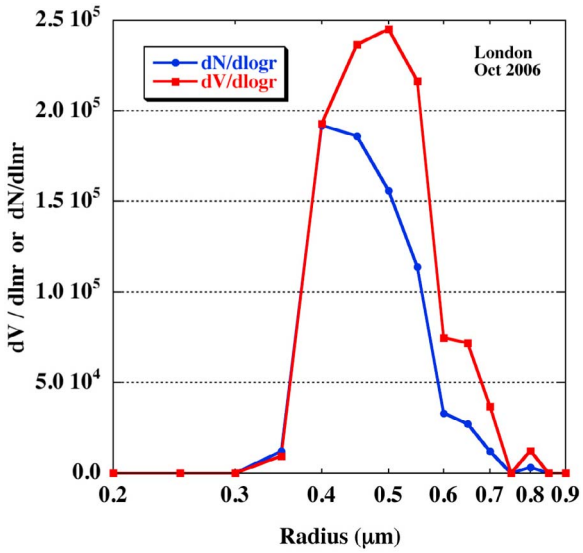

Figure 4. In situ measured ambient aerosol sizes associated with a fog event in London from *Dall'Osto et al.* [2009] (with additional conversion to volume distribution). These large submicron particles are composed of hydroxymethanesulphonate, which is a chemical species that is only formed in aqueous phase chemistry and therefore a tracer for aerosol processing by cloud or fog.

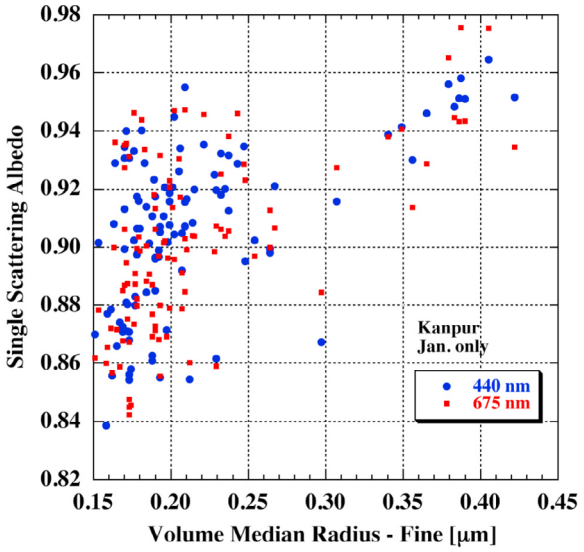

Figure 5. Almucantar retrievals of aerosol single scattering albedo (440 and 675 nm) versus fine mode volume median radius (in microns) at Kanpur, India, for January data only, for the interval 2002–2006.

870 nm. There was a tendency of SSA at 870 nm to be greater than at 440 nm as fine mode radius increased, owing to the combined effects of the size distributions, which primarily governs spectral scattering, and spectral variation of the imaginary refractive index, which strongly determines spectral absorption.

[13] The relationship between low-altitude cloud fraction (in conjunction with cloud optical depth; COD) and aerosol radius for dates where almucantar retrievals were made in January at Kanpur were investigated. Data from January of both 2003 and 2006 were selected since these years had the most cases with very large fine mode aerosol radius retrieved from AERONET. Figure 6 shows the product of the low cloud fraction (>600 mb cloud top pressure) times low cloud optical depth from the MODIS cloud algorithm [*Platnick et al.*, 2003] at the Terra satellite overpass time of midmorning. The retrieved radius values are from almucantar scans made after the fog/low cloud had dissipated, and are daily averages of all retrievals made in a given day. Figure 6 shows a rapid increase in accumulation mode aerosol radius as the low cloud fraction COD increases, consistent with fog/cloud processing of aerosol, since at higher low cloud optical depths and fractions it is likely that the fog layer is deeper and/or denser, thereby increasing the probability of cloud/fog droplet interaction with the aerosols over a greater vertical extent of the boundary layer. Since cloud optical depth was very low for some cases of high cloud fraction, the resulting relationship between cloud fraction and aerosol fine mode radius was noisy. The product of cloud fraction and COD resulted in a more rigorous way to investigate the interaction between cloud and aerosol, when relatively few observations were available for analysis. It is shown in Figure 6 that there are relatively few days when almucantar retrievals are made when low cloud was also identified by Terra MODIS in January of these years at Kanpur, thus emphasizing the difficulty in making almucantar retrievals during this month of high-frequency fog and/or cloud occurrence. The relatively low percentage of AERONET retrievals that show bimodality or large fine mode radius suggesting cloud processing at all AERONET sites in general is discussed in further detail in sections 4 and 5.

3.2. Arica, Chile

[14] The Arica AERONET site (18.47°S, 70.31°W, 25 m elevation) is located within less than 0.5 km of the Pacific Ocean coast in northern Chile in the small city of Arica (population ~200,000). Arica is situated ~140 km southeast from Ilo, Peru which is the location of a large copper smelter near to the coast, one of the largest single point sources of sulfur dioxide on Earth [see *Carn et al.*, 2007, and references therein]. The region of Arica, Ilo and the surrounding Atacama Desert is one of the driest on Earth, with extremely low annual rainfall (~0.8 mm average at Arica). Large emissions of SO_2 from Ilo have been observed from the Ozone Monitoring Instrument (OMI) satellite sensor [*Carn et al.*, 2007]. Most of the Peru coast and the central through northern Chilean coasts are adjacent to one of the largest and most seasonally persistent stratocumulus cloud fields in the world [*Klein and Hartmann*, 1993; *Bretherton et al.*, 2004]. *Kuang and Yung* [2000] have analyzed data from the Total Ozone Mapping Spectrometer (TOMS) on the Nimbus-7 satellite, showing higher stratocumulus cloud reflectance adjacent to Ilo and another near coastal smelter in Peru, thereby suggesting possible indirect aerosol effects of increased cloud droplet number, resulting in higher cloud albedo.

[15] *Chand et al.* [2010] measured aerosol properties further south on the Chilean coast (~25°S) at 690 m altitude and found that sulfate was the dominant identified submicron species, constituting 40% of the dry mass. For data

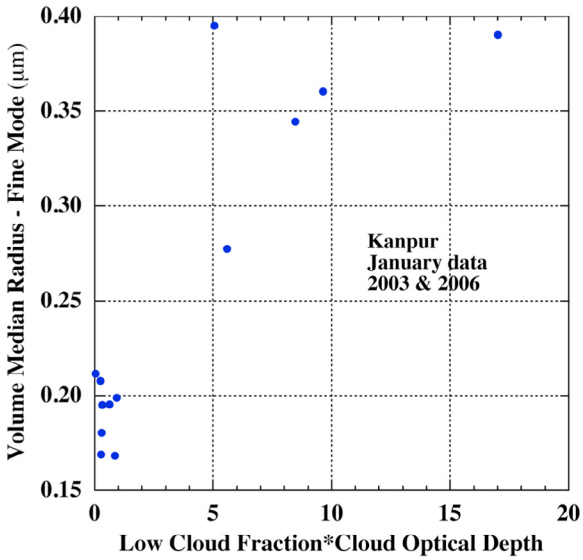

Figure 6. Product of low cloud fraction (cloud top pressure >600 mb) times low cloud optical depth from the MODIS cloud algorithm [*Platnick et al.*, 2003] at the Terra satellite overpass time (midmorning) at Kanpur versus the retrieved fine mode median radius (for January 2003 and 2006 only). The retrieved radius values are from almucantar scans made after the fog/low cloud had dissipated and are daily averages of all retrievals made in a given day.

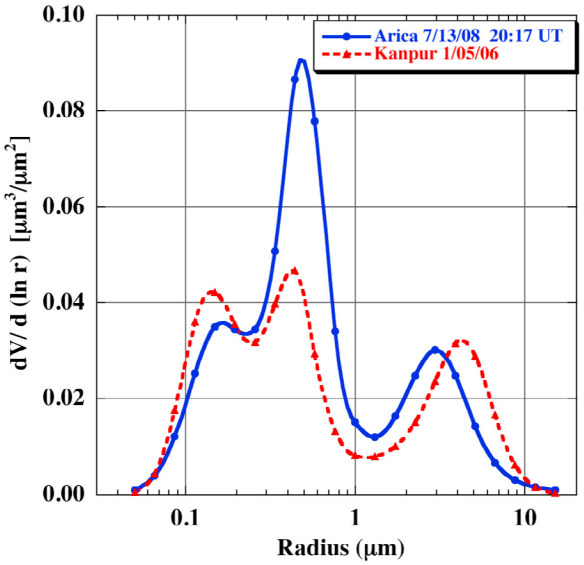

Figure 7. Almucantar retrieval made at Arica, Chile, on 13 July 2008 after the dissipation of the stratocumulus layer over the site. The 440 nm AOD during the almucantar scan averaged 0.58, and the $\alpha_{440-870}$ was 0.77. Similar to the size distribution retrievals at Kanpur (from Figure 3), Figure 7 shows a bimodal submicron size distribution at Arica with the largest of the two modes having a volume radius peak of ~0.48 μm.

sampled in situ from aircraft at 20°S westward off the coast of Chile in the marine stratocumulus region, *Allen et al.* [2011] found cloud droplet number well correlated with accumulation mode aerosol number and consistent with complete activation of 0.15 μm diameter number distribution accumulation mode aerosols.

[16] The marine stratocumulus cloud cover often overlays the Arica site in the morning and sometimes though the midafternoon, typically evaporating as the underlying land surface heats up. An example of an almucantar retrieval made after the dissipation of the stratocumulus layer over the site is shown in Figure 7. This case was observed on 13 July 2008, when cloud prevented direct Sun measurement of AOD until the last 2 h of the AERONET daily measurement sequence in late afternoon. The MODIS images on this date show 100% cloud cover with high visible reflectance over the ocean and Arica site at Terra overpass, and remaining similar over the ocean at Aqua overpass 3 h later, but evaporating over the land at that time. The 440 nm AOD during the almucantar scan averaged 0.58 and the $\alpha_{440-870}$ was 0.77. Similar to the size distribution retrievals at Kanpur shown in Figure 3, Figure 7 shows a bimodal submicron size distribution with the largest of the two modes having a volume radius peak of ~0.48 μm. The smaller of the two modes has a peak at ~0.16 μm, and the volume median radius of combined submicron modes is 0.33 μm. The larger of the two modes is likely the result of cloud processing of aerosol and the smaller possibly being composed of interstitial aerosol, or aerosol with no interaction with the cloud layer (such a aerosol above or below cloud top altitude). The coarse mode (supermicron radius) in this retrieval has an AOD of only ~0.03, which is nearly spectrally constant from 440 to 1020 nm, resulting in the AOD fine mode fraction of ~0.95 at 440 nm and ~0.91 at 870 nm. The retrieved single scattering albedo for this case is ~0.99 (also spectrally neutral), and therefore very weakly absorbing which is typical of most retrievals at Arica, where the average SSA is 0.98 for all wavelengths, from nearly 400 retrievals from 1998 to 2000, where AOD (440 nm) >0.4. This is consistent with the principal aerosol sources in the Arica region, as the SO_2 emissions from copper smelting create sulfate particles that are nonabsorbing [*Haywood and Boucher*, 2000] and both sea salt and marine biogenic sulfate particles (from dimethyl sulfide emission by phytoplankton) are also nonabsorbing.

[17] Several studies [*Reid et al.*, 1999; *Eck et al.*, 1999, 2001, 2003] have shown that there is significant curvature in the ln AOD versus ln λ relationship for fine mode–dominated aerosol size distributions, and that this curvature increases as submicron particle radius increases. The magnitude of the curvature is parameterized by $\alpha' = d\alpha/d \ln\lambda$ [*Eck et al.*, 1999] since there is typically a linear or near-linear relationship between Angstrom Exponent and ln λ, from the ultraviolet through near-infrared wavelengths. In Figure 8a we show the relationship between the almucantar retrieved volume median radius of the fine mode and the magnitude of α' computed from the 380 nm through 870 nm AOD measurements for all Arica retrievals made from 1998 to 2008. A zero value of α' means that there is no curvature and that the spectral AOD follow the linear or Angstrom relationship in ln AOD versus ln λ. Negative values of α' typically occur when a significant coarse mode optical depth fraction exits, while positive values occur for fine mode–dominated size distributions, with α' increasing as accumulation mode radius increases. The Arica retrieval shown in Figure 7 with the large cloud-processed mode has a large α' value of 1.49, indicating strong nonlinearity in the AOD spectra induced by large fine mode aerosols. Retrieved size distributions with submicron volume median radius of ~0.40 μm or higher are dominated by the cloud-processed particles and have little contribution from the smaller "interstitial" size accumulation mode aerosol (or aerosol that had no interaction with clouds, perhaps owing to differing altitude). Many of the retrievals with volume median radius range of 0.20–0.30 μm do not exhibit bimodality of the accumulation mode, but typically exhibit larger width of the fine mode (fine mode width increased as fine modal radius increased (correlation coefficient of 0.48)), including possibly more contribution of larger particles which may have interacted with cloud droplets. Figure 8b shows the scatterplot relationship between the aerosol optical depth and retrieved fine modal radius at Arica. There is an increasing trend of AOD at 440 nm as fine mode radius increases, with correlation coefficient (r) of 0.48. This trend may be due to several factors including an increase in coagulation rate as concentration increases [*Colarco et al.*, 2004], aerosol humidification, and also due to cloud processing of aerosols to larger sizes. When the particle number remains constant but the radius increases in the fine mode there is a resultant significant increase in AOD owing to an increase in light scattering efficiency. Of course many other factors influence the relationship shown in Figure 8b, such as aerosol concentrations, wind speed and resultant turbulent mixing, depth of the aerosol boundary

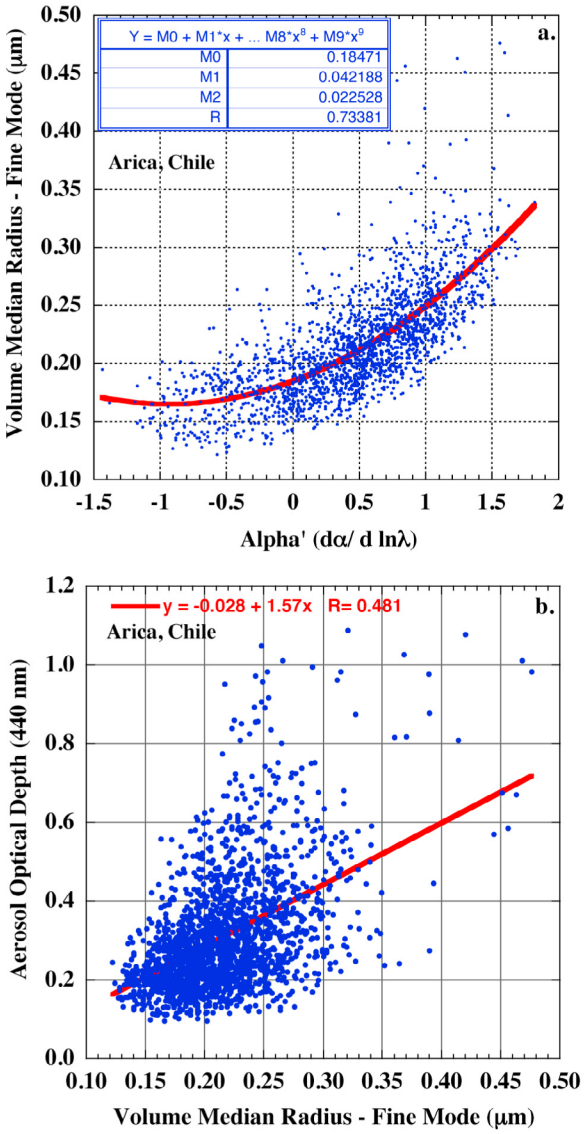

Figure 8. (a) Relationship between the almucantar-retrieved volume median radius of the fine mode and the magnitude of α' computed from the 380–870 nm AOD measurements for all Arica retrievals made from 1998 to 2008. A zero value of α' means that there is no curvature and that the spectral AOD follow the linear or Angstrom relationship in ln AOD versus ln λ. Positive values occur for fine mode–dominated size distributions, with α' increasing as accumulation mode radius increases. (b) Relationship between the aerosol optical depth and retrieved fine modal radius at Arica. There is an increasing trend of AOD at 440 nm as fine mode radius increases, with correlation coefficient (r) of 0.48.

layer, aging of the aerosol, and distance from aerosol sources, among others, which may partially account for the large amount of scatter in this plot.

[18] The relationship between aerosol fine mode radius from AERONET and cloud fraction as determined by MODIS satellite measurements at Arica was also investigated. Figure 9 shows the annual variation in the retrieved volume median radius and the low cloud fraction (>600 mb cloud top pressure) retrieved from the MODIS cloud algorithm with Terra satellite measurements. The MODIS cloud fraction is for a 1 by 1 degree latitude-longitude grid average with midpoint of 18.5°S 71.5°W, therefore all over ocean, directly to the west of Arica. All individual AERONET retrievals of fine mode radius from 1998 to 2008 are shown and the monthly mean low cloud fractions computed from 2001 to 2009 data are also depicted. The months of June through September exhibit the highest cloud fractions (>0.80) while the lowest fractions occurred during the months of January through March (<0.40). There is correspondingly similar seasonal trend in fine mode radius, which is most obvious in the lowest values over the annual cycle. This general coincidence of annual cycle in low cloud fraction and fine mode radius is consistent with the likelihood of cloud processing of the fine mode (largely sulfate) aerosol and/or humidification growth in the higher relative humidity environment in the vicinity of the clouds.

[19] The previously mentioned copper smelter at Ilo, Peru had a significant upgrade in January 2007 in order to decrease the emissions of sulfur dioxide. In Figure 10a, the time series of monthly mean AOD (500 nm) at Arica from 1998 to 2010 is shown, although a gap occurred in the data from April 2004 through May 2007 owing to a combination of logistics issues and technical problems. Figure 10b shows the daily average SO_2 mass column amounts measured by the OMI satellite instrument at Ilo, Peru [*Carn et al.*, 2007], from September 2004 through 2010. Note that the highest total column SO_2 were measured in 2006 through spring 2007, owing to the additional source of the Ubinas volcano eruptions upwind of Ilo. Unfortunately the AERONET data is missing when the smelter upgrade occurred in 2007;

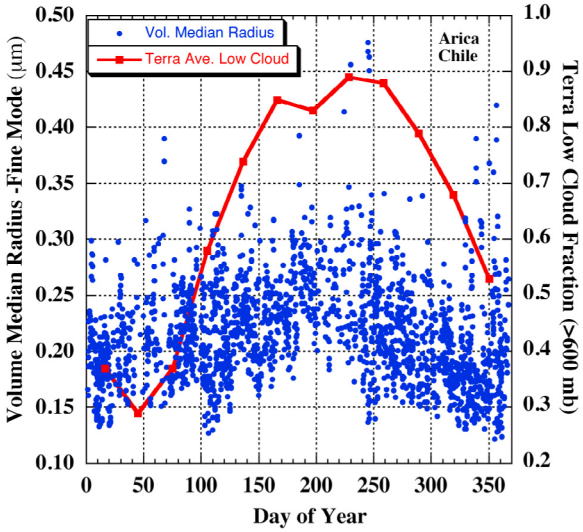

Figure 9. Annual variation in the retrieved volume median radius and the low cloud fraction (>600 mb cloud top pressure) retrieved from the MODIS cloud algorithm with Terra satellite measurements. The MODIS cloud fraction is for a 1 × 1 degree latitude-longitude grid average over the ocean directly to the west of Arica. All individual AERONET retrievals of fine mode radius from 1998 to 2008 are shown, and the monthly mean low cloud fractions computed from 2001 to 2009 data are depicted.

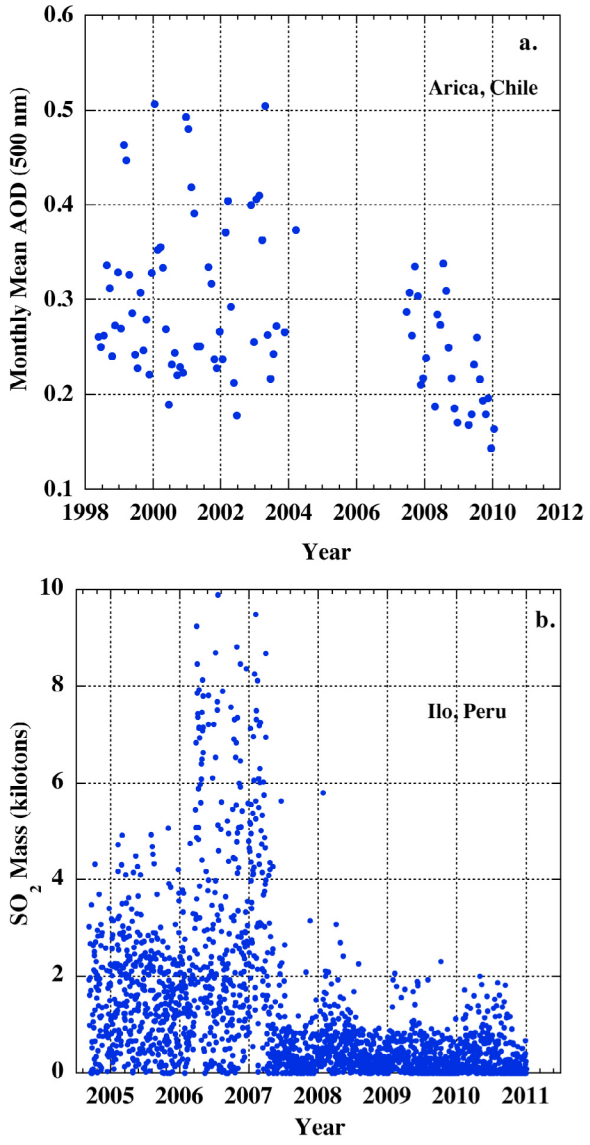

Figure 10. (a) Time series of the AERONET-measured monthly mean AOD (500 nm) at Arica, Chile, from 1998 to 2010, with a gap in the data from April 2004 through May 2007. (b) Daily average SO_2 mass column amounts measured by the OMI satellite instrument at Ilo, Peru [*Carn et al.*, 2007], from September 2004 through 2010. Note that the highest total column SO_2 measured in 2006 through spring 2007 was due to the additional source of the Ubinas volcano eruptions upwind of Ilo.

however, the significant decrease in AOD from May 2007 through January 2010 as compared to May 1998 through March 2004, strongly suggests that the ~90% reduction in emissions from this single major source has had a significant impact on the column integrated aerosol loading over the Arica site. There are only a few monthly mean AOD (500 nm) >0.3 after May 2007 and none greater than 0.4, when prior to April 2004 there were several months with relatively high AOD, including three months with ~0.5. Although the AOD exhibited a significant decrease, the fine mode radius does not show a significant change, with the linear regression showing a correlation coefficient (r) of only 0.10 (~1% of variance explained). Therefore it appears that the frequency of cloud processing and/or humidification of the aerosol over Arica may have remained relatively unchanged despite the significant drop in aerosol concentrations.

3.3. Fresno, California, USA

[20] The AERONET site in Fresno, California, is located near downtown Fresno, which is a city with a population of ~1 million located near the center of the wide San Joaquin Valley of central California. Thick radiation fog frequently forms in the late fall and winter (the rainy season) after the first significant rainfall. This fog often forms over a large area of the Central Valley bounded by the mountains of the Coast Ranges in the west and the Sierra Nevada to the east. Aerosol and aerosol precursor gases emitted in this region include urban, industrial, transportation and agricultural sources [*Chow et al.*, 2006]. Airborne high spectral resolution lidar data from February 2007 in the San Joaquin Valley [*Lewis et al.*, 2010] showed a shallow aerosol layer of ~1 km depth (constrained by temperature inversions), thereby increasing the likelihood that low-altitude cloud and especially fog may possibly interact with a significant fraction of the boundary layer aerosol in this region.

[21] Figure 11 is an Aqua MODIS image showing most of central California, adjacent Pacific Ocean and part of Nevada on 13 January 2004 at 21:10 UTC, with snow on the

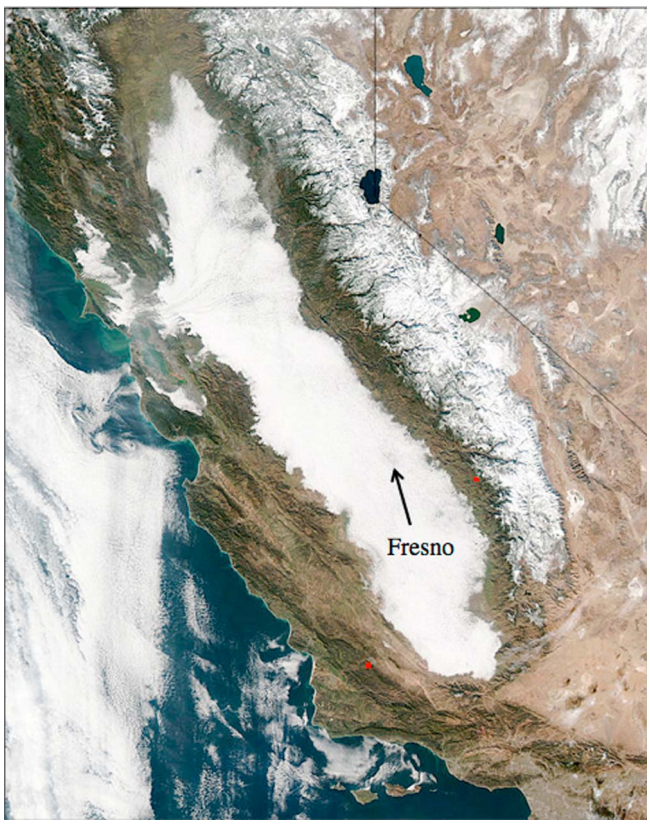

Figure 11. MODIS Aqua image from 13 January 2004 at 21:10 UTC showing extensive fog in the Central Valley of California; the location of Fresno is indicated. (Image courtesy of NASA/Goddard Space Flight Center Rapid Response.)

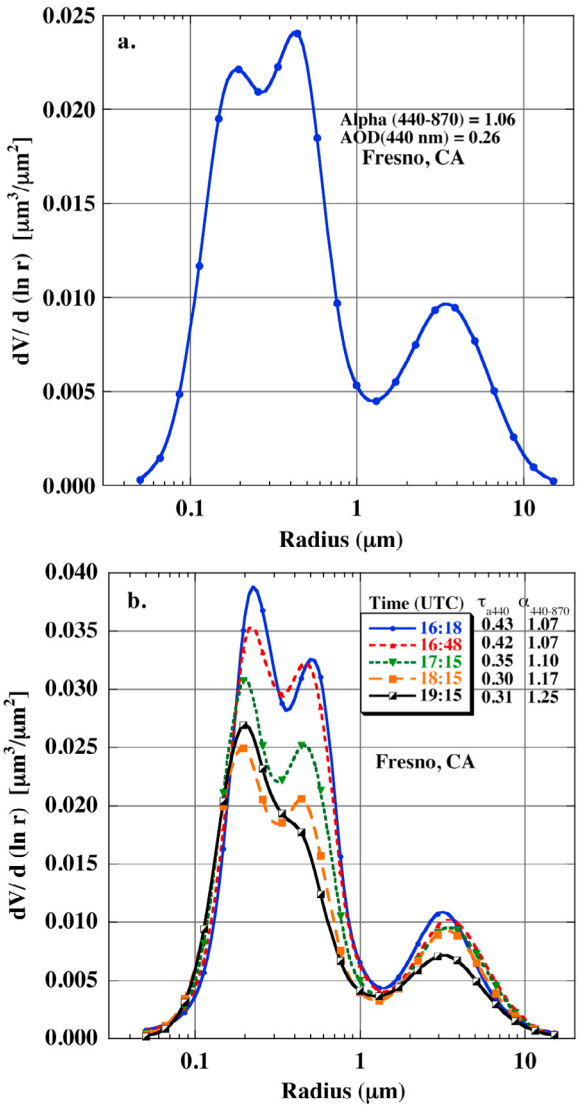

Figure 12. (a) Almucantar size distribution retrieval made at 23:32 UTC (75° solar zenith) on 13 January 2004 at Fresno from ~2.4 h after the MODIS image shown in Figure 11. (b) Size distribution retrievals from Fresno on the morning of 11 February 2006 over a time interval of ~3 h for these five almucantar scans.

ground over high elevations of the Sierra Nevada range. The majority of the Central Valley is covered in highly reflective fog or low cloud, and the location of Fresno is indicated on the image. Observations made at the Fresno airport on this date show cloud base at 75 m at 12:00 UTC (mist and 50% cloud), at 800 m (mist and 100% cloud) at 18:00 UTC and at 3000 m at 00:00 UTC on 14 January (haze and 30% cloud). AERONET observations showed cloud-free data for only the last hour of measurements of the day, and Figure 12a is the almucantar scan size distribution retrieval made at 23:32 UTC (75° solar zenith), from ~2.4 h after the MODIS image in Figure 11. The bimodal accumulation mode size distribution observed in Figure 12a is very similar to those observed in Kanpur and Arica, with the peak radius of the larger mode at ~0.43 μm and the peak radius of the smaller mode at ~0.19 μm (total median fine mode radius was 0.28 μm). The Angstrom exponent (440–870) is also similar (1.06) to that shown for the other cases, and the coarse mode aerosol optical depth determined from the retrieval is ~0.01, resulting in spectral fine mode fractions of the AOD of 0.96 at 440 nm and 0.92 at 870 nm. Several investigations [*Whiteaker and Prather*, 2003; *Rao and Collett*, 1995; *Jacob et al.*, 1989; *Munger et al.*, 1986] have measured the presence of hydroxymethanesulphonate in fog droplets and aerosols in the Central Valley of California in winter, and *Dixon and Aasen* [1999] measured aerosol HMS at other locations in the USA as well. As previously mentioned (Figure 4), HMS particles are a tracer for aqueous phase aerosol processing in fog or cloud droplets and are of a large size, ~0.4–0.5 micron radius. *Whiteaker and Prather* [2003] suggest that the formation rate of HMS increases as pH increases, reaching a maximum late in the lifetime of the fog and that the percentage of aerosol containing HMS reached a maximum of 40–50% following fog events at Bakersfield, California (also in the Central Valley). *Herckes et al.* [2007] measured high pH values in San Joaquin Valley fogs in winter, thus making them effective in oxidation of sulfur dioxide and for production of HMS. Measurements of the size distribution of ambient particles by *Whiteaker and Prather* [2003] showed a much higher frequency of particles containing HMS with aerodynamic radius greater than 0.35 μm (continuing to ~1 μm radius), therefore consistent with the measurements of HMS particle size made by *Dall'Osto et al.* [2009] in London. *Fahey et al.* [2005] in an analysis of San Joaquin Valley fog, simulated the mass size distribution of sulfate aerosol utilizing two different fog process models and found that the particle size distribution peaked at 0.38 μm radius, similar to in situ measurement results for ambient aerosols containing HMS.

[22] Size distribution retrievals showing bimodality on another date in Fresno, 11 February 2006, are shown in Figure 12b. The Fresno airport recorded mist at 12:00 UTC with 86% RH, and haze at 18:00 UTC with 64% RH (6 hourly report interval). The larger of the submicron modes (likely cloud processed) shows a peak radius decreasing from ~0.50 to ~0.45 μm, while the smaller mode also remained relatively constant at ~0.22 to ~0.19 μm (this slight decrease of the smaller mode may be related to decreasing RH) over the time interval of ~3 h for these 5 almucantar scans. Again the coarse mode (supermicron radius) AOD computed from these size distributions was small, ~0.01 (all wavelengths), therefore relatively insignificant optically. The 440 nm AOD decreased from ~0.43 at the time of the first scan shown to 0.31 at the time of the last scan, and the $\alpha_{440-870}$ increased from ~1.08 to 1.27. These observations show the temporal dissipation of the larger mode, which is consistent with estimates of the lifetime of HMS of a few hours after fog events [*Whiteaker and Prather*, 2003].

[23] All of the individual AERONET retrievals of fine mode radius made at Fresno are shown versus day of the year, from the time interval of 2002–2009, in Figure 13a. The majority of retrievals with fine mode median radius >0.20 μm occurred from November through mid-March. Also shown in Figure 13a is the monthly mean low cloud fraction from Terra MODIS (cloud top >600 mb), averaged over the 2001 through 2009 interval. The annual cycle of

low cloud fraction closely follows the annual cycle of fine mode radius with low cloud fraction from November through February ranging from ~0.25 to ~0.40, while in the summer months (June through September) the low cloud fraction is very small (~0.03–0.06). The coinciding occurrence of larger fine mode radius values with higher cloud fraction of low-altitude clouds from November through February is consistent with the possibility of fog/cloud processing and/or interaction. Of course other factors in addition to cloud processing are also likely to be responsible in part for the larger fine mode radius values in winter such as aerosol humidification at high relative humidity (which is enhanced in the higher-RH environment vicinity of clouds), and/or coagulation growth which increases as aerosol concentrations increase (Figure 13b shows somewhat higher AOD in winter months). In Figure 13c the relationship between fine mode radius and aerosol optical depth at 440 nm is shown for the months of November through February only. There is a significant trend of increasing AOD as fine mode radius increases (r = 0.64), which likely results partly from greater scattering efficiency as particle radius increases, in addition to possibly higher aerosol number concentrations being correlated with larger radius particles.

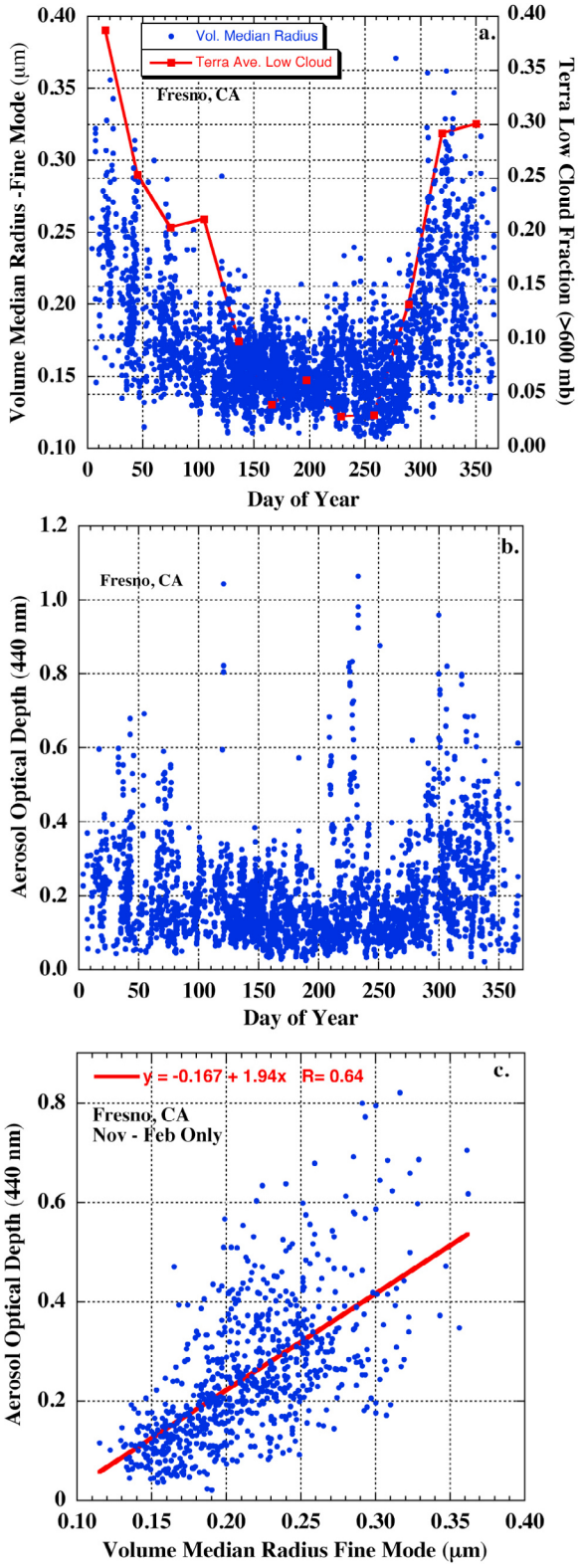

Figure 13. (a) All of the individual AERONET retrievals of fine mode radius made at Fresno versus day of the year for the time interval of 2002–2009. The majority of retrievals with fine mode median radius >0.20 μm occurred from November through mid-March. Also shown is the monthly mean low cloud fraction from Terra MODIS (cloud top >600 mb) averaged over the 2001 through 2009 interval. (b) AOD (440 nm) associated with all of the almucantar retrievals shown in Figure 13a. (c) Relationship between fine mode radius and aerosol optical depth at 440 nm at Fresno is shown for retrievals made during the months of November through February only.

3.4. Additional Sites

[24] Size distributions exhibiting a bimodal accumulation mode have been retrieved at some AERONET sites in eastern China, including Beijing, Xianghe (~60 km ESE of Beijing), and Taihu (~1000 km SSE of Beijing). Additionally, retrievals with large submicron radius that do not show a minimum between the two accumulation modes also occurred at the sites, and they have also been observed at the previously discussed sites. An example from the Beijing site on 24 January 2006 (05:28 UTC) is shown in Figure 14, where an obvious shoulder in the size distribution suggests a larger submicron mode with radius of ~0.4–0.5 μm, and a smaller fine mode of ~0.20 μm radius, and a total submicron radius of the two modes combined at 0.30 μm. The aerosol loading for this case was very high, with AOD (440 nm) of 2.87 and $\alpha_{440-870}$ of 1.04. The retrieved coarse mode (supermicron) AOD was nearly spectrally constant at ~0.05, therefore the resultant fine mode fraction of AOD was 0.98 at 440 nm and 0.96 at 870 nm. The MODIS Aqua satellite image (not shown) from ~1 h 20 min before this retrieval shows stratiform cloud in the immediate vicinity of the Beijing site and the grayish color of the cloud suggests that there are aerosols above cloud top altitude, thereby suggesting these nearest clouds are at a relatively low altitude. The study of *Niu et al.* [2010] found that the frequencies of fog events in wintertime over eastern-central China have doubled over the past three decades in response to changes in atmospheric circulation. This increase in fog

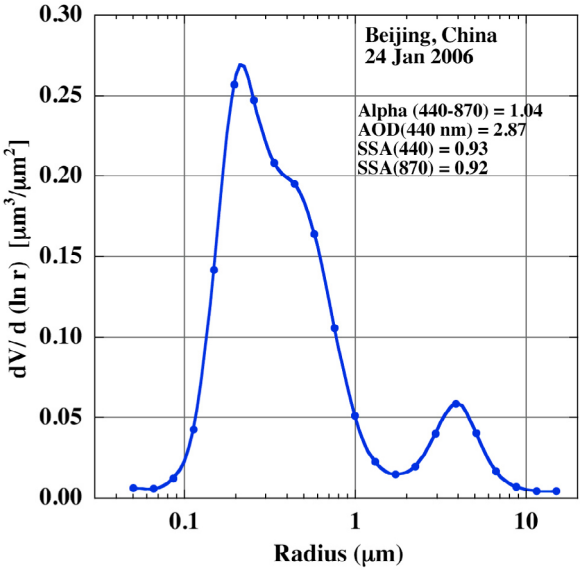

Figure 14. AERONET size distribution retrieval at the Beijing, China, site on 24 January 2006 at 05:28 UTC, with an obvious shoulder in the size distribution, suggesting a larger submicron mode with radius of ~0.4–0.5 μm, with a smaller fine mode of ~0.20 μm.

incidence in the region would likely result in increased probability of aerosol modification by fog processing. As previously mentioned, *Li et al.* [2011] made in situ measurements of aerosols under highly polluted conditions from Mt. Tai (~1.5 km altitude; ~420 km SSE of Beijing) and found that the cloud residue particles (or cloud-processed aerosols) had radius of ~0.40 μm (number distribution) that were approximately twice as large as the interstitial aerosols, or aerosols that did not interact with clouds. Also at Anmyon Island on the west coast of South Korea across the Yellow Sea from this region of China, some AERONET retrievals were identified with bimodal submicron size distributions, associated with clouds near the site. On one day, 15 November 2007, three retrievals within a 2 h interval showed a decrease in the larger accumulation mode with time, similar to that shown in Figure 12b at Fresno.

[25] Additional sites in Asia where AERONET bimodal accumulation mode size distributions retrievals occurred were located in Taiwan and continental Southeast Asia. Three sites in Taiwan (Chen Kung University, NCU Taiwan, and Taipei CWB) had some of these size distribution retrievals, suggesting cloud processing of aerosol. On one day, 3 March 2007, two sites near the west coast (within ~5–15 km of the ocean), Taipei CWB and Chen-Kung University (~260 km apart), showed similar bimodal fine mode retrievals (not shown) and the Terra and Aqua MODIS images showed extensive stratiform cloud over the waters of the Taiwan Strait to the west and also stratiform cloud to the east and north over the Pacific on that day. Therefore a large region in and near Taiwan may have been covered with this aerosol type on this date. In Southeast Asia, two sites in Thailand (Silpakorn, near to Bangkok; Chiang Mai Met Sta, in the north) and one in Vietnam (Bac Giang, in the north, near Hanoi) all have had a few cases of bimodal fine mode size distribution retrievals that have occurred in conditions of extensive nearby cloud cover.

[26] In Europe, AERONET sites located in the Po Valley and nearby valleys in northern Italy exhibited some retrievals showing bimodal accumulation mode size distributions. The AERONET site names are Ispra, Modena, Venise, and ISDGM_CNR located throughout the Po Valley region with Ispra in the west and Venice in the east (~307 km apart), with the Venise site located on a platform in the Adriatic Sea ~13 km east of Venice. These bimodal fine mode retrievals were also associated with nearby low-altitude fog or stratiform cloud (evident from MODIS images), thereby also suggesting cloud processing of the aerosol. An intensive field campaign to study primarily the fog and also the aerosols in this region was conducted in 1989, called "The Po Valley Fog Experiment 1989" [*Heintzenberg*, 1992; *Fuzzi et al.*, 1992]. During this field campaign, *Svenningsson et al.* [1992] measured the hygroscopic growth of ambient interstitial particles in the fog environment, and found that there were two general modes of accumulation size aerosol with different hygroscopic growth rates, with, on average, equal numbers of particles in each mode. Also from this same field experiment, *Noone et al.* [1992] presented in situ measurements of aerosol size distributions both prefog and during the fog events. Their measured volume size distribution radius values of the residual aerosol mode during these fog events peaked from ~0.30 to 0.35 μm, compared to the prefog peak radius of ~0.12 μm. These aerosol radii are similar in size (but somewhat smaller) to the AERONET retrieved radius values of ~0.4–0.5 μm for the cloud-processed or "residual" mode in this region, and the smaller fine mode retrieved radius is usually larger than 0.12 μm, typically ranging from ~0.15–0.20 μm. It is possible that variability in residual aerosol size is due in part from the number of cloud condensation-evaporation cycles and also from variation in ambient sulfur dioxide concentrations; however, this information is not available for assessment.

[27] Another region in Europe where a few retrievals of bimodal accumulation mode aerosols have been observed is ~40–60 km inland from the North Sea at the Lille site in northern France and at the Cabauw site in the Netherlands. Again, extensive stratiform clouds were apparent in MODIS images at times relatively close to the almucantar times of these "cloud-processed" aerosol cases.

[28] Very few cases of bimodal accumulation mode aerosol retrievals were identified from South American AERONET sites; however, measurements made in Sao Paulo, Brazil on 2 July 2007 provide a very informative case study. Figure 15a shows the MODIS Terra and Aqua images on this date, with stratiform cloud near the site at the Terra overpass time (13:00 UTC) and most of these clouds have evaporated by the time of the Aqua overpass (17:20 UTC), except along the coast and over the ocean. There were no direct Sun measurements of AOD acquired prior to ~12:00 UTC owing to cloud cover obscuring the Sun. Observations (3 hourly) from the weather station at Sao Paulo airport showed 100% cloud cover at 03:00 and 06:00 UTC and decreasing to 90% and 60% at 09:00 and 12:00 UTC, respectively, and no clouds at 15:00 UTC. These were clouds with low base altitude, ranging from 150 m at 03:00 UTC to 250 m at both 06:00 and 09:00 UTC and

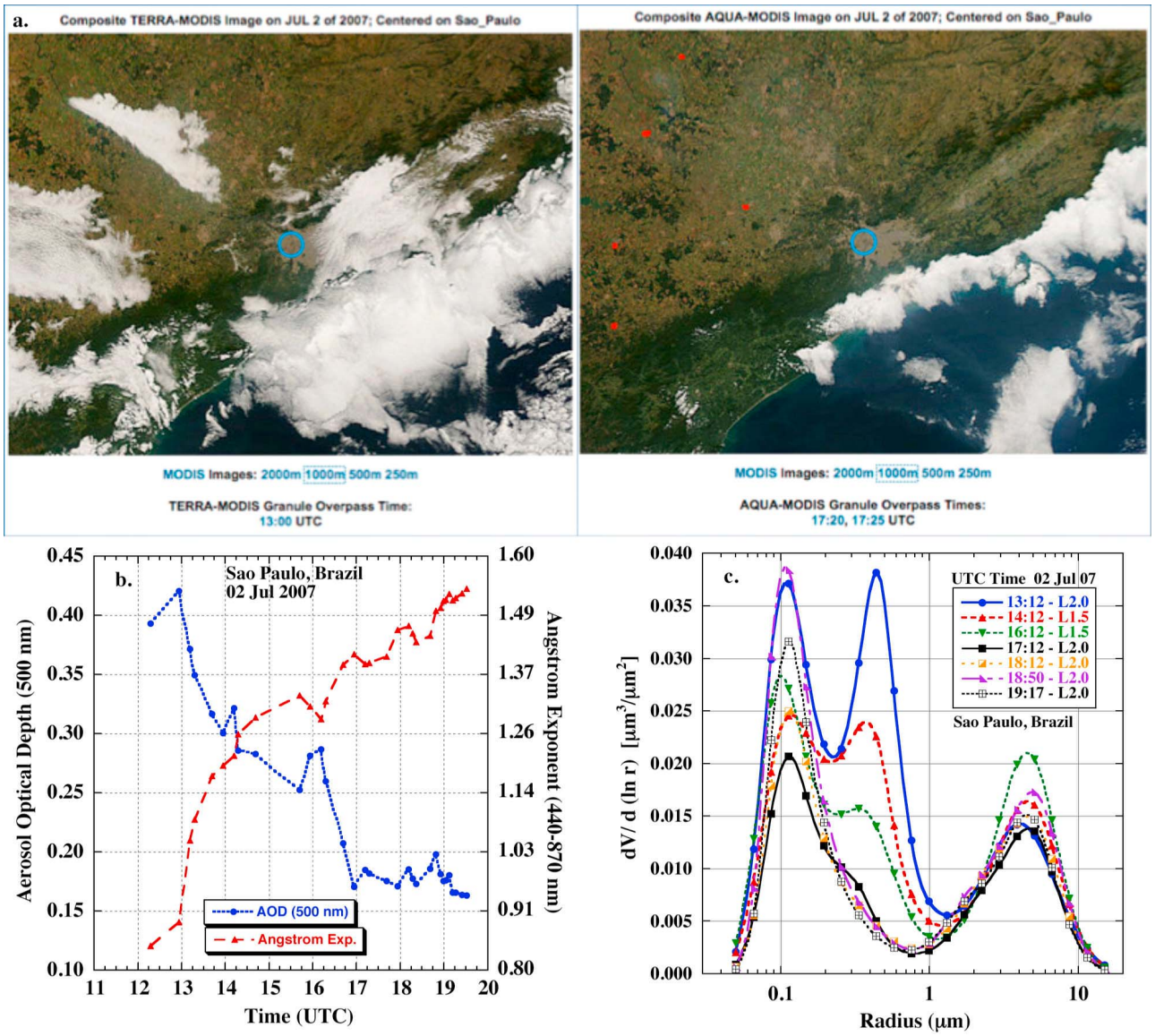

Figure 15. (a) MODIS Terra and Aqua images centered on the Sao Paulo, Brazil, site (blue circles) on 2 July 2007 with stratiform cloud near the site at the Terra overpass time (13:00 UTC) while most of these clouds have evaporated by the time of the Aqua overpass (17:20 UTC), except along the coast and over the ocean. (Image courtesy of NASA/Goddard Space Flight Center Rapid Response.) (b) Time series of the level 2.0 AOD (500 nm) and $\alpha_{440-870}$ for the complete day of observations on 2 July 2007, the date of the MODIS images shown in Figure 15a. (c) Aerosol volume size distribution retrievals made at Sao Paulo from ~13:00 to ~19:00 UTC (seven retrievals) on the same date.

450 m at 12:00 UTC. Surface relative humidity ranged from 86 to 89% from 06:00 to 12:00 UTC, falling to 62% at 15:00 UTC and 39% at 18:00 UTC. Figure 15b shows time series of the level 2.0 AOD (500 nm) and $\alpha_{440-870}$ for the complete day of observations with AOD shortly after cloud dissipation of ~0.40 and decreasing to ~0.16 by the end of the day. Angstrom exponent increased throughout the day, beginning at ~0.85 shortly after cloud dissipation and reaching a maximum of ~1.55 at the end of the day. The aerosol volume size distribution retrievals made from ~13:00 to ~19:00 UTC (7 retrievals) are shown in Figure 15c with all retrievals showing very low residual errors (<3.2%), computed from the comparison of measured to modeled sky radiances. Only the retrievals made at 14:12 and 16:12 UTC are not designated as level 2 because the solar zenith angles were less than 50 degrees (both ~49 degrees). The submicron radius size distributions show very large dynamics over the day during this 6 h time interval; however, the coarse mode size is relatively constant and the computed coarse mode AOD was relatively constant as well, ranging from ~0.011 to 0.015 (also nearly constant in wavelength). Bimodal submicron size distributions are evident for 3–4 h, with the earliest retrieval (13:12 UTC) showing the larger mode at ~0.44 μm and the smaller mode at ~0.11 μm. The radius of the smaller mode remains at ~0.11 μm while the larger mode radius

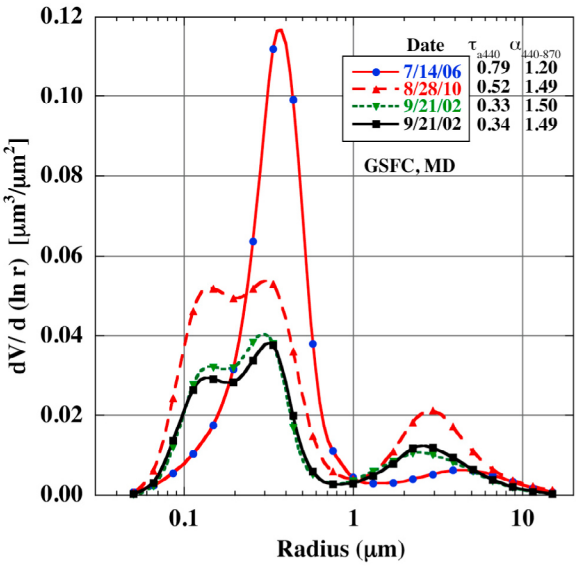

Figure 16. Retrievals from the Goddard Space Flight Center (GSFC), Maryland, site for 2 days with bimodal submicron size distributions, along with a retrieval exhibiting a single mode of very large submicron radius.

decreases to ~0.38 μm at 14:12 UTC and then to ~0.34 μm at 16:12 UTC. A hint of this larger mode remains at 17:12 UTC with a yet further reduced radius. This decrease in magnitude and shift in radius of the larger fine mode particles suggests dissipation and perhaps drying out of these aerosols after cloud dissipation and with RH continuing to decrease throughout the day. It is also possible that some advection of differing aerosol types may have occurred throughout the day, since winds of ~2–3 m/s blew from the northeast to east during this interval. However, these are relatively light horizontal winds so it is expected that much of the size distribution dynamics are likely to have occurred from aerosol interaction with clouds and also hygroscopic growth in the changing RH environment.

4. Discussion

[29] The primary focus of this paper is to examine volume size distribution retrievals that exhibit bimodality in the submicron radius size range for cases where stratiform clouds or fog have recently dissipated, thereby strongly suggesting aerosol-cloud interactions and cloud processing of aerosols. However, these types of retrievals are quite rare in the AERONET database in part since relatively cloud-free observations of sky radiance angular distributions are required over a large range of scattering angles to enable high-quality almucantar retrievals. Also, at the same time, a significant fraction of the total aerosols need to have been modified by interactions within the cloud environment in order for the column integrated size distribution to exhibit a separate size mode. This process may occur when low-altitude stratiform cloud and/or fog have vertical distributions that show significant overlap with the aerosol layer, and subsequently the cloud dissipates (evaporates) over a relatively large area. Therefore, although these types of retrievals are very rare (much less than 1% of retrievals), it seems likely that these types of cloud-processed aerosols are much more common than would be inferred from the very low frequency of such AERONET observations. If there is only partial dissipation of the cloud or fog, then some sky radiances remain cloud contaminated and the retrieval is not likely to be robust or even possible. Additionally, cloud processing and aerosol-cloud interactions also occur within cumulus type cloud environments and AERONET observations of cloud-processed aerosols for these types of cases are even more challenging to observe from almucantar scans. This is partly due to the previously mentioned cloud contamination issue for broken or scattered cumulus fields that precludes the ability to perform a robust retrieval. The aerosol field also needs to be spatially relatively uniform in order to achieve retrievals with small errors. Additionally, for cumulus cloud fields with less fractional coverage, and therefore more likely yielding a good retrieval (small error between measured and computed sky radiances), the fraction of the aerosol column that interacts with clouds is relatively small and therefore much less likely to exhibit a separate mode in a column integrated aerosol size distribution. Cumulus clouds over land (where most AERONET sites are located) also tend to have base altitudes that are often in the upper portion of the aerosol boundary layer thereby possibly limiting the potential for aerosol-cloud interaction, although vertical convection may offset this with aerosol transport in updrafts into cumulus clouds.

[30] An example of a site where very few observations of bimodal submicron mode size distribution retrievals have occurred is the Goddard Space Flight Center (GSFC) site in Greenbelt, Maryland in the mid-Atlantic region of the USA. The GSFC site is the AERONET intercalibration center and the reference Cimel instruments located there are calibrated at Mauna Loa Observatory thereby insuring highly accurate AOD (<0.005 in the visible and near IR) [*Eck et al.*, 1999]. Low-altitude stratiform clouds that are coincident in altitude with the aerosol layer and deep vertical extent fog are very rare at this site, although cumulus clouds are very common on days when almucantar retrievals are possible. Nearly continuous AERONET measurements have been made at the GSFC site for over 18 years as of the end of 2010, yet only 5 days were identified where submicron bimodal size distribution retrievals occurred. Retrievals from two of these days are shown in Figure 16, along with a retrieval exhibiting a single mode of very large submicron radius. The bimodal cases at GSFC exhibit less of a distinct larger mode (shallower minimum between modes) than most of the cases shown for previous sites and also at a somewhat smaller radius. The larger mode radius for these submicron bimodal cases ranged from ~0.30 to ~0.33 μm. Although smaller than the ~0.4–0.5 μm range of most of the retrievals presented in this paper, this radius range is also within the size range reported from some in situ measured and model computed cloud- or fog-processed aerosol sizes. All of these cases had time series of AOD on those dates that suggested significant cloud cover before and/or after the retrievals, owing to the lack of AOD measurements available. Additionally, the monomodal case shown from 14 July 2006 (AOD(440 nm) = 0.79) was the retrieval that had the largest computed fine mode volume median radius at the GSFC site, for the subset of data that had columnar water vapor amount (PW) exceeding 3 cm. The peak fine mode radius on this

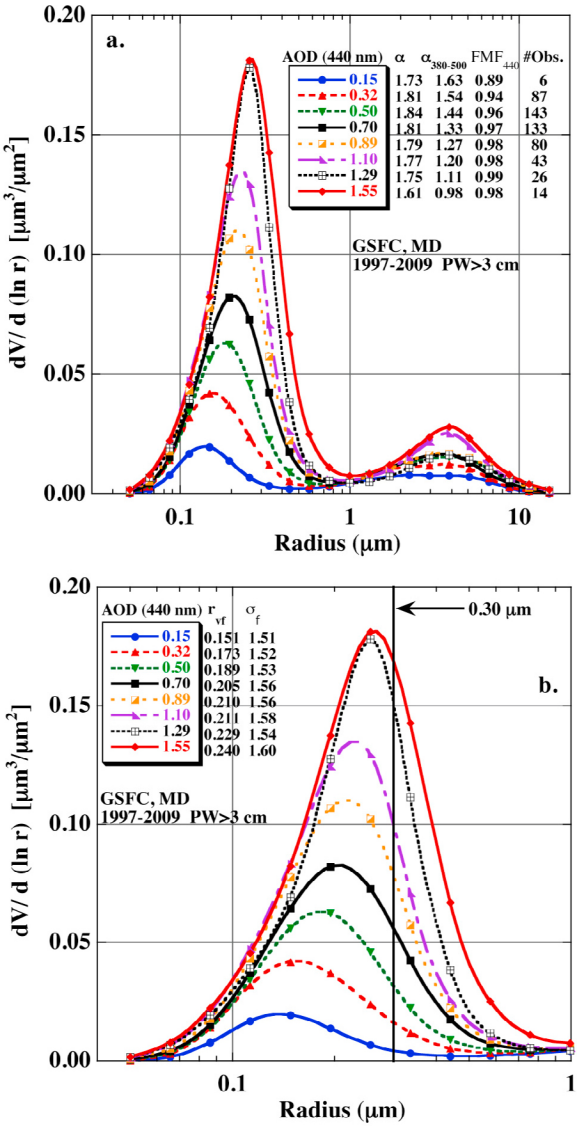

Figure 17. (a) Climatological average size distributions at the Goddard Space Flight Center (GSFC) site from 1997 to 2009 as a function of 440 nm AOD. These are a subset of the complete set of level 2 size distributions where columnar water vapor amount (precipitable water (PW)) exceeds 3 cm. (b) Enlargement of the fine mode only from Figure 17a.

date was 0.37 μm, and there was also much cloud cover in the region as evidenced by both missing AOD for the entire two previous days (all data were cloud screened) and at ~30 min after this scan was taken in the early morning and other times during the day, and from extensive regional cloud cover in the Terra MODIS image at ~4 h after the retrieval time. The $\alpha_{440-870}$ for this case was 1.20, and the AOD spectra was also very nonlinear as parameterized by $\alpha' = 1.79$ (a very high value), therefore consistent with very large fine mode aerosol size. It is noted that two other secondary reference instruments located at GSFC on this date and time retrieved essentially the same size distribution as from the primary reference, shown in Figure 16.

[31] The climatological average size distributions as a function of AOD level for the GSFC site are shown in Figure 17. These are a subset of the complete set of level 2 size distributions when columnar water vapor amount (precipitable water, PW) exceeds 3 cm. This threshold of high water vapor amount effectively excludes cases when smoke has been transported to the GSFC site, sometimes from distant sources as was shown in the work of *Eck et al.* [2003]. Days with high PW are also more likely to have higher relative humidity and cloud cover than days with low PW. The average size distributions at all AOD levels in Figure 17 are dominated by the fine mode, with the fine mode fraction of AOD at 440 nm ranging from 0.89 to 0.99, and computed coarse mode AOD of ~0.02 at all wavelengths. The fine mode, shown isolated in Figure 17b, clearly exhibits an increase in radius as AOD increases throughout the measured range of AOD. The average fine mode volume median radius increased steadily from ~0.15 μm at AOD (440 nm) = 0.15 to a radius of 0.24 μm at AOD (440 nm) = 1.55. Since all of these retrievals were made under high PW conditions it is assumed that the relative humidity did not vary over a very wide range as a function of AOD. Therefore the observed increase in fine mode radius as AOD increased may have largely resulted from aerosol coagulation since coagulation rate increases as concentration increases [*Reid et al.*, 1998]. However, humidification may still have been significant in conjunction with cloud interaction or in the high-humidity halo surrounding clouds, especially since U.S. mid-Atlantic coast aerosol is strongly hygroscopic [*Kotchenruther et al.*, 1999]. In conjunction with the increase in radius there was also a general trend of increasing average width of the size distribution as AOD increased. An increase in the width of the fine mode distribution that occurred as aerosol concentrations increased may possibly have been caused by mixtures of larger aged aerosols combined with freshly emitted or recently formed smaller particles (from gas to particle conversion). *Thornhill et al.* [2008] analyzed aircraft in situ measurements of volume size distribution for the U.S. East Cost and Midwestern region and found significantly larger particles (and greater width) at higher altitude (2–4 km) than from the surface to 2 km, perhaps owing to more aging and cloud interaction at higher altitudes. Additionally, at GSFC, aerosol-cloud interactions may have resulted in some increase in the larger tail or shoulder of the fine mode distribution (the 0.3 μm radius line is denoted in Figure 17 as a general marker of large and therefore possibly cloud-processed accumulation size aerosol). As the AOD increases in the mid-Atlantic region of the United States it is highly probable that an increasing fraction of the aerosols are aged from one to several days. *Lelieveld and Heintzenberg* [1992] utilized estimates of cloud fraction and lifetimes to infer that globally the average sulfate particle goes through 3 to 7 cloud condensation-evaporation events over its average 1 week lifetime before removal from the atmosphere. Although it is beyond the scope of this paper to investigate this possibility, it was suggested by *Jeong and Li* [2010], from analysis of AERONET AOD in conjunction with cloud fraction data at a site in Oklahoma, that the increase of AOD in the vicinity of clouds was likely caused by cloud processing of aerosols more than from aerosol humidification.

[32] It is noted that the size distributions in Figure 17 for the GSFC site differ from those presented for the same site in

the work of *Dubovik et al.* [2002], hereafter D02. This is due to improvements made to the retrievals in version 2 (V2) versus the pre–version 1 retrievals used in D02 (see *Eck et al.* [2008] for a brief discussion of V2). The width (geometric standard deviation) of the fine mode for the GSFC site in D02 is significantly narrower at 1.46 (compared to ∼1.51 to 1.60 in V2), and was also constant as a function of AOD. Additionally, the fine mode volume median radius values in D02 differ somewhat from those shown in Figure 17, being smaller at lower AOD and larger at the highest AOD levels than V2. This is not a result of the data shown here being only those retrievals for which PW >3, since very similar values of median radius and width occur when all the version 2 GSFC retrievals are analyzed, regardless of PW level. The aerosol absorption for the GSFC site is slightly greater in V2 for the data where AOD (440 nm) >0.4, with average imaginary refractive index at ∼0.004 versus ∼0.003 in D02. This results in average SSA being 0.01 lower than in D02, at 0.97, 0.96, 0.95, and 0.94 at the wavelengths 440, 675, 870 and 1020 nm, respectively.

5. Summary and Conclusions

[33] The largest radius fine mode (submicron radius)–dominated aerosol size distributions retrieved from AERONET almucantar scans have been observed after fog or cloud dissipation events. These types of column-integrated size distributions have been observed at several AERONET sites in many regions of the world after evaporation of low-altitude cloud such as stratocumulus or fog (essentially cloud with base at ground level). These cases with "cloud-processed" aerosol are sometimes bimodal in the accumulation mode with the large-size mode often at ∼0.4–0.5 μm radius (volume distribution); the smaller mode typically at ∼0.12 to ∼0.20 μm may be interstitial aerosol that were not modified by incorporation in droplets and/or aerosol that are less hygroscopic in nature. The smaller mode may also result from aerosols that were at altitudes above (or below) cloud layers, thereby not interacting with clouds. Bimodal accumulation mode size distributions have often been observed with in situ measurements of aerosols that have interacted with clouds.

[34] In situ measurements of ambient aerosols after fog dissipation (e.g., London, England and the San Joaquin Valley, California) have shown particles in the same or similar size range (modal peak at ∼0.4–0.5 μm volume distribution radius) that are composed of hydroxymethanesulphonate (HMS), which are formed exclusively in the aqueous phase within cloud or fog droplets. Additional in situ measurements of large-size aerosol (submicron radius) have also been made in eastern China, and the Po Valley, Italy associated with cloud processing of aerosol. Therefore AERONET aerosol size distribution retrievals, made after dissipation of cloud and/or fog, are in good agreement with particle sizes measured by in situ techniques for cloud-processed aerosols.

[35] The number of AERONET retrievals where a bimodal submicron size distribution is observed, including a cloud-processed mode, is a very small percentage of the total retrievals. This is due in part to the requirement of nearly cloudless conditions for the range of angular sky radiances needed for a good retrieval. This is characteristic of the biases of remote sensing measurements of aerosol properties toward conditions of low cloud fraction, both from ground and satellite sensors. Additionally a significant portion of the aerosol layer and cloud/fog layer needs to be coincident in order for the aerosol-cloud interactions to occur over a large enough fraction of the aerosol loading to be able to observe a separate mode in column-integrated size distributions. Since AOD was observed to increase as fine radius increased, the sampling bias of cloud-processed aerosols in the near-cloud environment likely results in an underestimation of total AOD from most satellite and ground based remote sensing observations, and therefore underestimation of aerosol direct radiative forcing.

[36] It is also noted that these types of fine mode bimodal size distributions have only been observed from AERONET retrievals in polluted conditions in regions where sulfate is known to be a significant aerosol species. There have been no cases of bimodal submicron size distributions observed in regions and seasons when biomass-burning aerosols dominate, possibly owing in part to the less soluble and less hygroscopic nature of biomass burning aerosols and also possibly owing to the types of clouds and their relative altitude with respect to the smoke layers in these regions.

[37] Aerosols of this type and large size range may also be formed by cloud processing in partly cloudy conditions in lower concentrations and may contribute to the "shoulder" of larger-size particles in the accumulation mode retrievals, especially in regions where sulfate or other highly soluble aerosol are a significant component of the total aerosol composition.

[38] **Acknowledgments.** The AERONET project was supported by Michael D. King, retired in 2008 from the NASA EOS project office, and by Hal B. Maring, Radiation Sciences Program, NASA Headquarters. The IIT Kanpur AERONET site was operational since January 2001 under a joint agreement between IIT Kanpur and NASA. We acknowledge the efforts of Harish Vishwakarama in the operation of this AERONET site. M. Rivas acknowledges support by UTA-Mayor grant 4721 (2011–2012). H. Chen acknowledges support by MOST grant 2010CB950804 (2010–2014).

References

Albrecht, B. A. (1989), Aerosols, cloud microphysics, and fractional cloudiness, *Science*, *245*, 1227–1230, doi:10.1126/science.245.4923.1227.

Alkezweeny, A. J. (1995), Field observations of in-cloud nucleation and the modification of atmospheric aerosol-size distributions after cloud evaporation, *J. Appl. Meteorol.*, *34*, 2649–2654, doi:10.1175/1520-0450(1995)034<2649:FOOICN>2.0.CO;2.

Allen, G., et al. (2011), Southeast Pacific atmospheric composition and variability sampled along 20°S during VOCALS-Rex, *Atmos. Chem. Phys.*, *11*, 5237–5262, doi:10.5194/acp-11-5237-2011.

Badarinath, K. V. S., S. K. Kharol, A. R. Sharma, and P. S. Roy (2009), Fog over Indo-Gangetic Plains—A study using multi-satellite data and ground observations, *IEEE J. Selec. Topics Appl. Earth Obs. Remote Sens.*, *2*(3), 185–195, doi:10.1109/JSTARS.2009.2019830.

Baxla, S. P., A. A. Roy, T. Gupta, S. N. Tripathi, and R. Bandyopadhyaya (2009), Analysis of diurnal and seasonal variation of submicron outdoor aerosol mass and size distribution in a northern Indian city and its correlation to black carbon, *Aerosol Air Qual. Res.*, *9*, 458–469.

Bretherton, C. S., T. Uttal, C. W. Fairall, S. E. Yuter, R. A. Weller, D. Baumgardner, K. Comstock, R. Wood, and G. B. Raga (2004), The epic 2001 stratocumulus study, *Bull. Am. Meteorol. Soc.*, *85*, 967–977, doi:10.1175/BAMS-85-7-967.

Carn, S. A., A. J. Krueger, N. A. Krotkov, K. Yang, and P. F. Levelt (2007), Sulfur dioxide emissions from Peruvian copper smelters detected by the Ozone Monitoring Instrument, *Geophys. Res. Lett.*, *34*, L09801, doi:10.1029/2006GL029020.

Chand, D., D. A. Hegg, R. Wood, G. E. Shaw, D. Wallace, and D. S. Covert (2010), Source attribution of climatically important aerosol properties

measured at Paposo (Chile) during VOCALS, *Atmos. Chem. Phys.*, *10*, 10,789–10,801, doi:10.5194/acp-10-10789-2010.

Chinnam, N., S. Dey, S. N. Tripathi, and M. Sharma (2006), Dust events in Kanpur, northern India: Chemical evidence for source and implications to radiative forcing, *Geophys. Res. Lett.*, *33*, L08803, doi:10.1029/2005GL025278.

Chow, J. C., L.-W. A. Chen, J. G. Watson, D. H. Lowenthal, K. A. Magliano, K. Turkiewicz, and D. E. Lehrman (2006), PM2.5 chemical composition and spatiotemporal variability during the California Regional PM10/PM2.5 Air Quality Study (CRPAQS), *J. Geophys. Res.*, *111*, D10S04, doi:10.1029/2005JD006457.

Clarke, A. D., et al. (2002), INDOEX aerosol: A comparison and summary of chemical, microphysical, and optical properties observed from land, ship, and aircraft, *J. Geophys. Res.*, *107*(D19), 8033, doi:10.1029/2001JD000572.

Colarco, P. R., M. R. Schoeberl, B. G. Doddridge, L. T. Marufu, O. Torres, and E. J. Welton (2004), Transport of smoke from Canadian forest fires to the surface near Washington, D. C.: Injection height, entrainment, and optical properties, *J. Geophys. Res.*, *109*, D06203, doi:10.1029/2003JD004248.

Dall'Osto, M., R. M. Harrison, H. Coe, and P. Williams (2009), Real-time secondary aerosol formation during a fog event in London, *Atmos. Chem. Phys.*, *9*, 2459–2469, doi:10.5194/acp-9-2459-2009.

Das, S. K., A. Jayaraman, and A. Misra (2008), Fog-induced variations in aerosol optical and physical properties over the Indo-Gangetic Basin and impact to aerosol radiative forcing, *Ann. Geophys.*, *26*, 1345–1354, doi:10.5194/angeo-26-1345-2008.

Dey, S., S. N. Tripathi, R. P. Singh, and B. N. Holben (2004), Influence of dust storms on the aerosol optical properties over the Indo-Gangetic basin, *J. Geophys. Res.*, *109*, D20211, doi:10.1029/2004JD004924.

Dixon, R. W., and H. Aasen (1999), Measurement of hydroxymethanesulfonate in atmospheric Aerosols, *Atmos. Environ.*, *33*, 2023–2029, doi:10.1016/S1352-2310(98)00416-6.

Dubovik, O., and M. D. King (2000), A flexible inversion algorithm for the retrieval of aerosol optical properties from Sun and sky radiance measurements, *J. Geophys. Res.*, *105*, 20,673–20,696, doi:10.1029/2000JD900282.

Dubovik, O., A. Smirnov, B. N. Holben, M. D. King, Y. J. Kaufman, T. F. Eck, and I. Slutsker (2000), Accuracy assessments of aerosol optical properties retrieved from AERONET Sun and sky-radiance measurements, *J. Geophys. Res.*, *105*, 9791–9806, doi:10.1029/2000JD900040.

Dubovik, O., B. N. Holben, T. F. Eck, A. Smirnov, Y. J. Kaufman, M. D. King, D. Tanre, and I. Slutsker (2002), Variability of absorption and optical properties of key aerosol types observed in worldwide locations, *J. Atmos. Sci.*, *59*, 590–608, doi:10.1175/1520-0469(2002)059<0590:VOAAOP>2.0.CO;2.

Dubovik, O., et al. (2006), Application of spheroid models to account for aerosol particle nonsphericity in remote sensing of desert dust, *J. Geophys. Res.*, *111*, D11208, doi:10.1029/2005JD006619.

Eck, T. F., B. N. Holben, J. S. Reid, O. Dubovik, A. Smirnov, N. T. O'Neill, I. Slutsker, and S. Kinne (1999), Wavelength dependence of the optical depth of biomass burning, urban, and desert dust aerosols, *J. Geophys. Res.*, *104*, 31,333–31,349, doi:10.1029/1999JD900923.

Eck, T. F., B. N. Holben, D. E. Ward, O. Dubovik, J. S. Reid, A. Smirnov, M. M. Mukelabai, N. C. Hsu, N. T. O'Neill, and I. Slutsker (2001), Characterization of the optical properties of biomass burning aerosols in Zambia during the 1997 ZIBBEE Field Campaign, *J. Geophys. Res.*, *106*, 3425–3448, doi:10.1029/2000JD900555.

Eck, T. F., B. N. Holben, J. S. Reid, N. T. O'Neill, J. S. Schafer, O. Dubovik, A. Smirnov, M. A. Yamasoe, and P. Artaxo (2003), High aerosol optical depth biomass burning events: A comparison of optical properties for different source regions, *Geophys. Res. Lett.*, *30*(20), 2035, doi:10.1029/2003GL017861.

Eck, T. F., et al. (2008), Spatial and temporal variability of column-integrated aerosol optical properties in the southern Arabian Gulf and United Arab Emirates in summer, *J. Geophys. Res.*, *113*, D01204, doi:10.1029/2007JD008944.

Eck, T. F., et al. (2010), Climatological aspects of the optical properties of fine/coarse mode aerosol mixtures, *J. Geophys. Res.*, *115*, D19205, doi:10.1029/2010JD014002.

Fahey, K. M., S. N. Pandis, J. L. Collett Jr., and P. Herckes (2005), The influence of size-dependent droplet composition on pollutant processing by fogs, *Atmos. Environ.*, *39*, 4561–4574, doi:10.1016/j.atmosenv.2005.04.006.

Fuzzi, S., et al. (1992), The Po Valley Fog Experiment 1989, *Tellus, Ser. B*, *44*, 448–468, doi:10.1034/j.1600-0889.1992.t01-4-00002.x.

Gautam, R., N. C. Hsu, M. Kafatos, and S.-C. Tsay (2007), Influences of winter haze on fog/low cloud over the Indo-Gangetic plains, *J. Geophys. Res.*, *112*, D05207, doi:10.1029/2005JD007036.

Gautam, R., Z. Liu, R. P. Singh, and N. C. Hsu (2009), Two contrasting dust-dominant periods over India observed from MODIS and CALIPSO data, *Geophys. Res. Lett.*, *36*, L06813, doi:10.1029/2008GL036967.

Hansen, J., M. Sato, and R. Ruedy (1997), Radiative forcing and climate response, *J. Geophys. Res.*, *102*, 6831–6864, doi:10.1029/96JD03436.

Haywood, J., and O. Boucher (2000), Estimates of the direct and indirect radiative forcing due to tropospheric aerosols: A review, *Rev. Geophys.*, *38*, 513–543, doi:10.1029/1999RG000078.

Hegg, D. A., D. S. Covert, H. Jonsson, D. Khelif, and C. A. Friehe (2004), Observations of the impact of cloud processing on aerosol light-scattering efficiency, *Tellus, Ser. B*, *56*, 285–293.

Heintzenberg, J. (1992), The Po Valley Fog Experiment 1989: What have we learned, where do we go from here?, *Tellus, Ser. B*, *44*, 443–447, doi:10.1034/j.1600-0889.1991.t01-3-00002.x-i1.

Herckes, P., H. Chang, T. Lee, and J. L. Collett Jr. (2007), Air pollution processing by radiation fogs, *Water Air Soil Pollut.*, *181*, 65–75, doi:10.1007/s11270-006-9276-x.

Holben, B. N., et al. (1998), AERONET—A federated instrument network and data archive for aerosol characterization, *Remote Sens. Environ.*, *66*, 1–16, doi:10.1016/S0034-4257(98)00031-5.

Holben, B. N., T. F. Eck, I. Slutsker, A. Smirnov, A. Sinyuk, J. Schafer, D. Giles, and O. Dubovik (2006), AERONET's version 2.0 quality assurance criteria, *Proc. SPIE Int. Soc. Opt. Eng.*, *6408*, 64080Q, doi:10.1117/12.706524.

Hoppel, W., G. Frick, J. Fitzgerald, and R. Larson (1994), Marine boundary layer measurements of new particle formation and the effects nonprecipitating clouds have on aerosol size distribution, *J. Geophys. Res.*, *99*, 14,443–14,459, doi:10.1029/94JD00797.

Intergovernmental Panel on Climate Change (IPCC) (2007), *Climate Change 2007: The Physical Science Basis, Contribution of Working Group I to the Fourth Assessment Report of the Intergovernmental Panel on Climate Change*, edited by S. Solomon et al., Cambridge Univ. Press, New York.

Jacob, D. J., E. W. Gottlieb, and M. J. Prather (1989), Chemistry of a polluted cloudy boundary layer, *J. Geophys. Res.*, *94*, 12,975–13,002, doi:10.1029/JD094iD10p12975.

Jenamani, R. K. (2007), Alarming rise in fog and pollution causing a fall in maximum temperature over Delhi, *Curr. Sci.*, *93*, 314–322.

Jeong, M.-J., and Z. Li (2010), Separating real and apparent effects of cloud, humidity, and dynamics on aerosol optical thickness near cloud edges, *J. Geophys. Res.*, *115*, D00K32, doi:10.1029/2009JD013547.

Johnson, B. T., and S. R. Osborne (2011), Physical and optical properties of mineral dust aerosol measured by aircraft during the GERBILS campaign, *Q. J. R. Meteorol. Soc.*, *137*, 1117–1130, doi:10.1002/qj.777.

Klein, S. A., and D. L. Hartmann (1993), The seasonal cycle of low stratiform clouds, *J. Clim.*, *6*, 1587–1606, doi:10.1175/1520-0442(1993)006<1587:TSCOLS>2.0.CO;2.

Koren, I., Y. J. Kaufman, L. A. Remer, and J. V. Martins (2004), Measurement of the effect of Amazon smoke on inhibition of cloud formation, *Science*, *303*, 1342–1345, doi:10.1126/science.1089424.

Kotchenruther, R., P. Hobbs, and D. Hegg (1999), Humidification factors for atmospheric aerosols off the mid-Atlantic coast of the United States, *J. Geophys. Res.*, *104*, 2239–2251, doi:10.1029/98JD01751.

Kuang, Z., and Y. L. Yung (2000), Reflectivity variations off the Peru Coast: Evidence for indirect effect of anthropogenic sulfate aerosols on clouds, *Geophys. Res. Lett.*, *27*, 2501–2504, doi:10.1029/2000GL011376.

Lelieveld, J., and J. Heintzenberg (1992), Sulfate cooling effect on climate through in-cloud oxidation of anthropogenic SO_2, *Science*, *258*, 117–120, doi:10.1126/science.258.5079.117.

Lewis, J., R. De Young, R. Ferrare, and D. A. Chu (2010), Comparison of summer and winter California Central Valley aerosol distributions from lidar and MODIS measurements, *Atmos. Environ.*, *44*, 4510–4520, doi:10.1016/j.atmosenv.2010.07.006.

Li, W., P. Li, G. Sun, S. Zhou, Q. Yuan, and W. Wang (2011), Cloud residues and interstitial aerosols from non-precipitating clouds over an industrial and urban area in northern China, *Atmos. Environ.*, *45*, 2488–2495, doi:10.1016/j.atmosenv.2011.02.044.

Lu, M.-L., W. Jian, R. C. Flagan, J. H. Seinfeld, A. Freedman, R. A. McClatchey, and H. H. Jonsson (2003), Analysis of humidity halos around trade wind cumulus clouds, *J. Atmos. Sci.*, *60*, 1041–1059, doi:10.1175/1520-0469(2003)60<1041:AOHHAT>2.0.CO;2.

Munger, J. W., C. Tiller, and M. R. Hoffmann (1986), Identification of hydroxymethanesulfonate in fog water, *Science*, *231*, 247–249, doi:10.1126/science.231.4735.247.

Niu, F., Z. Li, C. Li, K.-H. Lee, and M. Wang (2010), Increase of wintertime fog in China: Potential impacts of weakening of the eastern Asian monsoon circulation and increasing aerosol loading, *J. Geophys. Res.*, *115*, D00K20, doi:10.1029/2009JD013484.

Noone, K. J., et al. (1992), Changes in aerosol size and phase distributions due to physical and chemical processes in fog, *Tellus, Ser. B*, *44*, 489–504, doi:10.1034/j.1600-0889.1992.t01-4-00004.x.

Novakov, T., M. O. Andreae, R. Gabriel, T. W. Kirchstetter, O. L. Mayol-Bracero, and V. Ramanathan (2000), Origin of carbonaceous aerosols over the tropical Indian Ocean: Biomass burning or fossil fuels?, *Geophys. Res. Lett.*, *27*, 4061–4064, doi:10.1029/2000GL011759.

Platnick, S., M. D. King, S. A. Ackerman, W. P. Menzel, B. A. Baum, J. C. Riédi, and R. A. Frey (2003), The MODIS cloud products: Algorithms and examples from terra, *IEEE Trans. Geosci. Remote Sens.*, *41*, 459–473, doi:10.1109/TGRS.2002.808301.

Prasad, A. K., and R. P. Singh (2007), Changes in aerosol parameters during major dust storm events (2001–2005) over the Indo-Gangetic Plains using AERONET and MODIS data, *J. Geophys. Res.*, *112*, D09208, doi:10.1029/2006JD007778.

Prasad, A. K., R. P. Singh, and M. Kafatos (2006), Influence of coal based thermal power plants on aerosol optical properties in the Indo-Gangetic basin, *Geophys. Res. Lett.*, *33*, L05805, doi:10.1029/2005GL023801.

Pueschel, R. F., P. B. Russell, D. A. Allen, G. V. Ferry, K. G. Snetsinger, J. M. Livingston, and S. Verma (1994), Physical and optical properties of the Pinatubo volcanic aerosol: Aircraft observations with impactors and a Sun-tracking photometer, *J. Geophys. Res.*, *99*, 12,915–12,922, doi:10.1029/94JD00621.

Radke, L. F., and P. V. Hobbs (1991), Humidity and particle fields around some small cumulus clouds, *J. Atmos. Sci.*, *48*, 1190–1193, doi:10.1175/1520-0469(1991)048<1190:HAPFAS>2.0.CO;2.

Rao, X., and J. L. Collett Jr. (1995), Behavior of S(IV) and formaldehyde in a chemically heterogeneous cloud, *Environ. Sci. Technol.*, *29*, 1023–1031, doi:10.1021/es00004a024.

Reid, J., P. Hobbs, R. Ferek, D. Blake, J. Martins, M. Dunlap, and C. Liousse (1998), Physical, chemical, and optical properties of regional hazes dominated by smoke in Brazil, *J. Geophys. Res.*, *103*, 32,059–32,080, doi:10.1029/98JD00458.

Reid, J., T. F. Eck, S. A. Christopher, P. V. Hobbs, and B. N. Holben (1999), Use of the Angstrom exponent to estimate the variability of optical and physical properties of aging smoke particles in Brazil, *J. Geophys. Res.*, *104*, 27,473–27,489, doi:10.1029/1999JD900833.

Reid, J., R. Koppmann, T. Eck, and D. Eleuterio (2005), A review of biomass burning emissions, Part II: Intensive physical properties of biomass burning particles, *Atmos. Chem. Phys.*, *5*, 799–825.

Reid, J., B. Brooks, K. K. Crahan, D. A. Hegg, T. F. Eck, N. O'Neill, G. de Leeuw, E. A. Reid, and K. D. Anderson (2006), Reconciliation of coarse mode sea-salt aerosol particle size measurements and parameterizations at a subtropical ocean receptor site, *J. Geophys. Res.*, *111*, D02202, doi:10.1029/2005JD006200.

Reid, J., E. A. Reid, A. Walker, S. Piketh, S. Cliff, A. Al Mandoos, S.-C. Tsay, and T. F. Eck (2008), Dynamics of southwest Asian dust particle size characteristics with implications for global dust research, *J. Geophys. Res.*, *113*, D14212, doi:10.1029/2007JD009752.

Schmid, B., J. Michalsky, R. Halthore, M. Beauharnois, L. Harrison, J. Livingston, P. Russell, B. Holben, T. Eck, and A. Smirnov (1999), Comparison of aerosol optical depth from four solar radiometers during the fall 1997 ARM intensive observation period, *Geophys. Res. Lett.*, *26*, 2725–2728, doi:10.1029/1999GL900513.

Singh, R. P., S. Dey, S. N. Tripathi, V. Tare, and B. Holben (2004), Variability of aerosol parameters over Kanpur, northern India, *J. Geophys. Res.*, *109*, D23206, doi:10.1029/2004JD004966.

Smirnov, A., B. N. Holben, T. F. Eck, O. Dubovik, and I. Slutsker (2000), Cloud screening and quality control algorithms for the AERONET data base, *Remote Sens. Environ.*, *73*, 337–349, doi:10.1016/S0034-4257(00)00109-7.

Su, W., G. L. Schuster, N. G. Loeb, R. R. Rogers, R. A. Ferrare, C. A. Hostetler, J. W. Hair, and M. D. Obland (2008), Aerosol and cloud interaction observed from high spectral resolution lidar data, *J. Geophys. Res.*, *113*, D24202, doi:10.1029/2008JD010588.

Svenningsson, I. B., H.-C. Hansson, A. Wiedensohler, J. A. Ogren, K. J. Noone, and A. And Hallberg (1992), Hygroscopic growth of aerosol particles in the Po Valley, *Tellus, Ser. B*, *44*, 556–569, doi:10.1034/j.1600-0889.1992.t01-1-00009.x.

Tackett, J. L., and L. Di Girolamo (2009), Enhanced aerosol backscatter adjacent to tropical trade wind clouds revealed by satellite-based lidar, *Geophys. Res. Lett.*, *36*, L14804, doi:10.1029/2009GL039264.

Tare, V., et al. (2006), Measurements of atmospheric parameters during Indian Space Research Organization Geosphere Biosphere Program Land Campaign II at a typical location in the Ganga Basin: 2. Chemical properties, *J. Geophys. Res.*, *111*, D23210, doi:10.1029/2006JD007279.

Thornhill, K. L., et al. (2008), The impact of local sources and long-range transport on aerosol properties over the northeast U.S. region during INTEX-NA, *J. Geophys. Res.*, *113*, D08201, doi:10.1029/2007JD008666.

Tripathi, S. N., et al. (2006), Measurements of atmospheric parameters during Indian Space Research Organization Geosphere Biosphere Programme Land Campaign II at a typical location in the Ganga basin: 1. Physical and optical properties, *J. Geophys. Res.*, *111*, D23209, doi:10.1029/2006JD007278.

Twohy, C. H., J. A. Coakley, and W. R. Tahnk (2009), Effect of changes in relative humidity on aerosol scattering near clouds, *J. Geophys. Res.*, *114*, D05205, doi:10.1029/2008JD010991.

Twomey, S. (1977), The influence of pollution on the shortwave albedo of clouds, *J. Atmos. Sci.*, *34*, 1149–1152, doi:10.1175/1520-0469(1977)034<1149:TIOPOT>2.0.CO;2.

Várnai, T., and A. Marshak (2011), Global CALIPSO observations of aerosol changes near clouds, *IEEE Geosci. Remote Sens. Lett.*, *8*, 19–23, doi:10.1109/LGRS.2010.2049982.

Venkataraman, C., G. Habib, A. Eiguren-Fernandez, A. H. Miguel, and S. K. Friedlander (2005), Residential biofuels in South Asia: Carbonaceous aerosol emissions and climate, *Science*, *307*, 1454–1456, doi:10.1126/science.1104359.

Whiteaker, J. R., and K. A. Prather (2003), Hydroxymethanesulfonate as a tracer for fog processing of individual aerosol particles, *Atmos. Environ.*, *37*, 1033–1043, doi:10.1016/S1352-2310(02)01029-4.

Zhang, Q., and X. Tie (2011), High solubility of SO_2: Evidence in an intensive fog event measured in the NCP region, China, *Atmos. Chem. Phys. Discuss.*, *11*, 2931–2947, doi:10.5194/acpd-11-2931-2011.

G. T. Arnold, T. F. Eck, D. M. Giles, B. N. Holben, N. A. Krotkov, S. Platnick, J. S. Schafer, A. Sinyuk, and A. Smirnov, NASA Goddard Space Flight Center, Greenbelt, MD 20771, USA. (thomas.f.eck@nasa.gov)

A. Arola, Finnish Meteorological Institute, FI-70211 Kuopio, Finland.

P. Artaxo, Institute of Physics, University of São Paulo, São Paulo 05508-090, Brazil.

C. J. Bruegge, NASA Jet Propulsion Laboratory, Pasadena, CA 91109, USA.

S. A. Carn, Department of Geological and Mining Engineering and Sciences, Michigan Technological University, Houghton, MI 49931, USA.

H. Chen, Chinese Academy of Sciences, Beijing 100101, China.

O. Dubovik and P. Goloub, Laboratoire d'Optique Atmospherique, CNRS, Universite de Lille, F-59655 Villeneuve d'Ascq, France.

J. S. Reid, Naval Research Laboratory, 7 Grace Hopper St., Monterey, CA 93907, USA.

M. A. Rivas, Laboratorio de Radiación Solar Ultravioleta, Departamento de Física, Facultad de Ciencias, Universidad de Tarapacá, Casilla 7-D, Arica, Chile.

R. P. Singh, School of Earth and Environmental Sciences, Chapman University, Orange, CA 92866, USA.

S. N. Tripathi, Department of Civil Engineering, Indian Institute of Technology Kanpur, Kanpur 20816, India.